ELSEVIER

Chemical Geology 152 (1998) 227–256

CHEMICAL GEOLOGY
INCLUDING
ISOTOPE GEOSCIENCE

The thermal and cementation histories of a sandstone petroleum reservoir, Elk Hills, California Part 1: $^{40}Ar/^{39}Ar$ thermal history results

Keith I. Mahon *, T. Mark Harrison, Marty Grove

Department of Earth and Space Sciences and Institute of Geophysics and Planetary Physics, University of California, Los Angeles, CA 90095-1567, USA

Received 8 August 1997; revised 18 June 1998; accepted 18 June 1998

Abstract

Recent developments in K-feldspar $^{40}Ar/^{39}Ar$ thermochronometry have provided new tools to deal with interpretive impediments that previously limited its application to investigating sedimentary basin thermal histories. These new methodologies were applied to detrital K-feldspars recovered at various depths from a deep well drilled through a carbonate-cemented sandstone petroleum reservoir in the southern San Joaquin Valley, California. Thermal histories obtained from both thermochronological analysis and burial history constraints were used to constrain a conductive heat flow model of basin evolution. The basin appears to have experienced a broadly linear heating history due to burial throughout the early and middle Miocene followed by a significant increase in heating rate between 9 and 6 Ma. In a companion paper [Mahon, K.I., Harrison, T.M., McKeegan, K.D., 1998. The thermal and cementation histories of a sandstone petroleum reservoir, Elk Hills, California. Part 2: In situ oxygen and carbon isotopic results. Chem. Geol. 152, 257–271], we apply the thermal model to predict the temperature evolution of the much shallower late Miocene Stevens sands, a prolific petroleum producer. Ratios of excess ^{40}Ar to chlorine calculated from the differential release of radiogenic and nucleogenic argon during isothermal heating steps indicate a uniform value of $5.4 \pm 0.9 \times 10^{-5}$ over the 2.5 km vertical distance separating the samples from well 934-29R suggesting that the basin receives a high basal flux of radiogenic argon.

Keywords: Elk Hills field; Kern County, California; Ar-40/Ar-39; Thermal history; Noble gas; Alkali feldspar

1. Introduction

The formation, migration, and storage of liquid hydrocarbons are largely dictated by the thermal history of the source rock and the cementation history of the reservoir. Understanding the thermal history permits assessment of whether source rocks have experienced conditions appropriate for petroleum formation. The mobility of hydrocarbons and their storage capacity in clastic reservoirs are a direct consequence of porosity and permeability modifications due to diagenetic reactions, which are generally dominated by the dissolution of detrital phases and precipitation of cements. Since these

* Corresponding author. Exxon Production Research Company, P.O. 2189, Houston, TX 77252-2189, USA. Tel.: +1 713 431 7036.

0009-2541/98/$ - see front matter
PII: S0009-2541(98)00115-6

reactions occur over a range of burial depths and temperatures, a complete evaluation of reservoir modification through diagenesis also requires knowledge of the temperature history.

Several approaches have been developed to assess sedimentary basin thermal histories, including use of vitrinite reflectance (Teichmüller, 1958), apatite fission tracking dating (e.g., Gleadow et al., 1983), and the $^{40}Ar/^{39}Ar$ step-heating of K-feldspar (e.g., Harrison and Bé, 1983). The latter two methods are based on the degree to which products of radioactive decay have reequilibrated due to elevated temperatures during burial, and as such have the practical benefit of yielding absolute timing information. $^{40}Ar/^{39}Ar$ dating of detrital K-feldspar was first applied to the evaluation of basin thermal histories by Harrison and Bé (1983) using rocks from the southern San Joaquin basin. However, poor laboratory controls and the degradation of the low-temperature portion of the age spectrum by excess ^{40}Ar ($^{40}Ar_E$) resulted in only crude thermal history estimates (Harrison and Burke, 1988). Two recent developments in the $^{40}Ar/^{39}Ar$ step-heating method, the multi-diffusion domain model (Lovera et al., 1989) and correction of Cl-correlated $^{40}Ar_E$ (Harrison et al., 1994), potentially overcome these limitations. This paper, and its companion (Mahon et al., 1998), revisit the San Joaquin basin for the purpose of constraining cementation history of the Stevens sands, an important petroleum reservoir in the region.

Wood and Boles (1991) described an approach that potentially permits the time-dependent storage capacity of partially cemented petroleum reservoirs to be determined. Assuming a model evolution for the oxygen isotope composition of the pore fluid, they calculated temperatures of cementation from measured oxygen isotope compositions of calcite cements using known water–mineral fractionation thermometers (e.g., Friedman and O'Neil, 1977). They then estimated the timing of cementation by

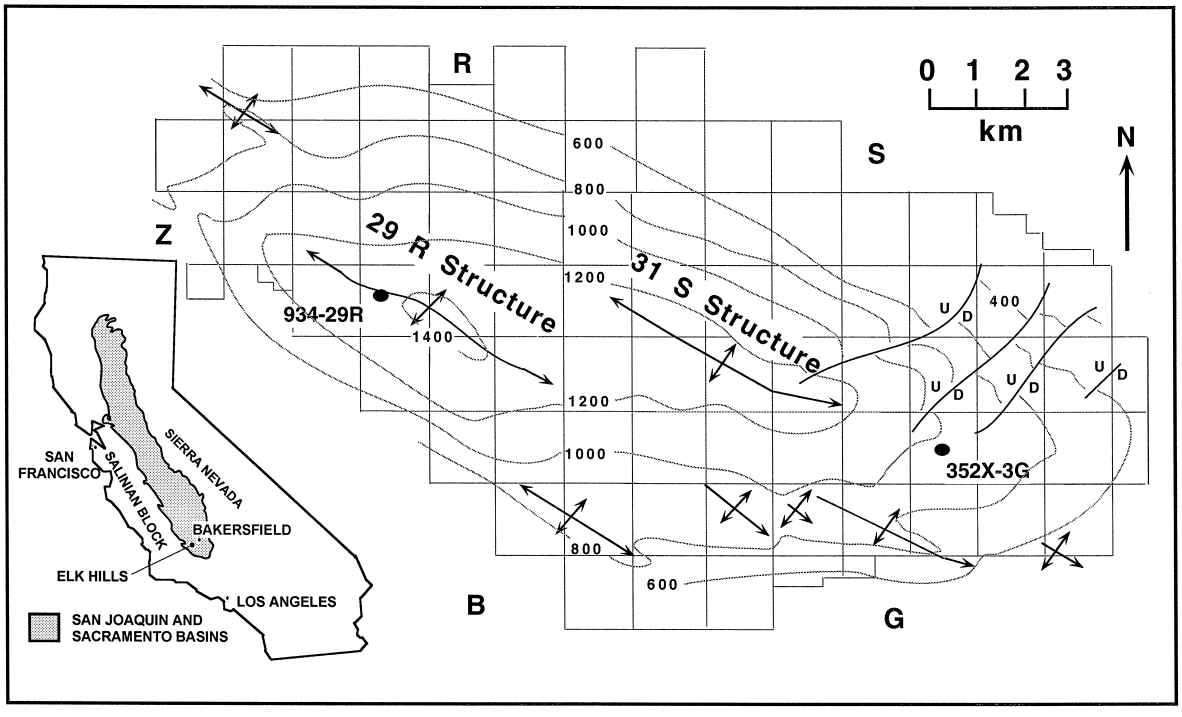

Fig. 1. Boundaries of the Naval Petroleum Reserve no. 1 at Elk Hills, California (modified from Nicholson, 1990). San Joaquin basin location map shown in the inset. Structural contours of the top of the Tulare B limestone are in feet above sea level. Also shown are the traces of anticlines 29R and 31S and locations of wells 934-29R (used in this study) and 352X-3G (used in the companion study). Normal faults shown in the lower right dip to the southeast (U = footwall, D = hanging wall).

coupling this information with a thermal history derived largely from stratigraphic controls.

We identified the Naval Petroleum Reserve Number 1 (NPR-1) at Elk Hills, southern San Joaquin Valley, CA (Fig. 1), as an appropriate environment to test the approach outlined by Wood and Boles (1991). The NPR-1 oil field contains the deepest drill hole in California (7445 m) and thus, provides access to a wide spectrum of stratigraphic levels and ambient temperatures. Furthermore, it is adjacent the North Coles Levee oil field, the site of the Wood and Boles (1991) study. The Stevens sandstone, a Miocene arkosic turbidite present in both oil fields, is a prolific oil reservoir and is largely calcite cemented.

In this paper we describe the geological setting of the basin and the methods used to recover thermal histories from $^{40}Ar/^{39}Ar$ step-heating experiments of detrital K-feldspars from arkosic sections intersected by deep drill holes. We then use these data to constrain a conductive heat flow model of basin evolution. In the companion paper (Mahon et al., 1998), we obtain in situ ion microprobe oxygen and carbon isotopic measurements of carbonate cements that yield, respectively, temperature estimates of cementation and insights into the source of pore fluids. The goal is to test the feasibility of combining thermochronological information with in situ stable isotope thermometry to estimate the age of cementation events and thus, assess the evolution of porosity, permeability, and pore fluid composition in the petroleum reservoir.

2. Geological setting

The Stevens sands, late Miocene turbidites within the Monterey formation (Fig. 2), are an important petroleum producing interval in the eastern portion of Elk Hills (Reid, 1990b; Wood and Boles, 1991). Although our ultimate goal is to understand the diagenetic history of this unit, a problem with restricting our focus to these strata is that the peak estimated temperatures within the Stevens sands at Elk Hills are $< 100°C$ (Fishburn, 1990). Since temperatures of $\sim 150°C$ are required to induce measurable loss of argon from even the smallest diffusion domains typical in basement K-feldspars (see Lovera et al., 1997), it is not possible to constrain thermal histories using $^{40}Ar/^{39}Ar$ results from K-feldspar within the depth range of the Stevens sands. However, arkosic sandstones encountered several kilometers below the Stevens horizon (Fig. 2) have measured borehole temperatures in the range 150° to 200°C (Fishburn, 1990) and as such are suitable candidates for K-feldspar $^{40}Ar/^{39}Ar$ thermochronological analysis. Therefore, we chose to utilize samples recovered from this temperature range to constrain the temperature–time history of the shallower intervals.

The San Joaquin basin (Fig. 1) began to form in the late Cretaceous as a forearc basin and continued as a major depocenter following the development of the San Andreas transform system throughout the late Cenozoic. During the late Miocene, the Salinian block was emplaced to the west of the southern San Joaquin basin, partially isolating the basin (Graham and Williams, 1985; Bent, 1988). An amalgamation of sands and organic shales, derived largely from adjacent denuded batholiths of mostly Cretaceous age in the south, east, and west, were deposited together in the vicinity of Elk Hills via submarine fans (Reid, 1990b). Anoxic conditions in the deep marine setting were ideal for the preservation of organic-rich source rocks.

East of the San Andreas fault, the deformational pattern grades from proximal transpression to a fold and thrust belt developed at greater distances (Lowell, 1972; Nicholson, 1990; Fig. 2). The Elk Hills oil field, situated within the transition zone, is characterized by transpressional deformation overprinted by high angle reverse faulting (Nicholson, 1990). This deformation began at Elk Hills during the latest Miocene and profoundly affected turbidite depositional patterns. Uplift in the Elk Hills region is restricted to development of antiformal structures during the Pleistocene (Jones and Gillespie, 1995) with the magnitude of erosion limited to less than a few 100's of meters. Structure contours constructed for the top of the Pleistocene Tulare B limestone reveal two southeasterly trending, left-stepping, en echelon folds, locally termed 29R and 31S (Fig. 1). A northwesterly plunging anticline dominates below ~ 2100 m. At Elk Hills, this latter feature is juxtaposed against 31S and 29R by a left-lateral, strike slip fault (Maher et al., 1975; Nicholson, 1990). To

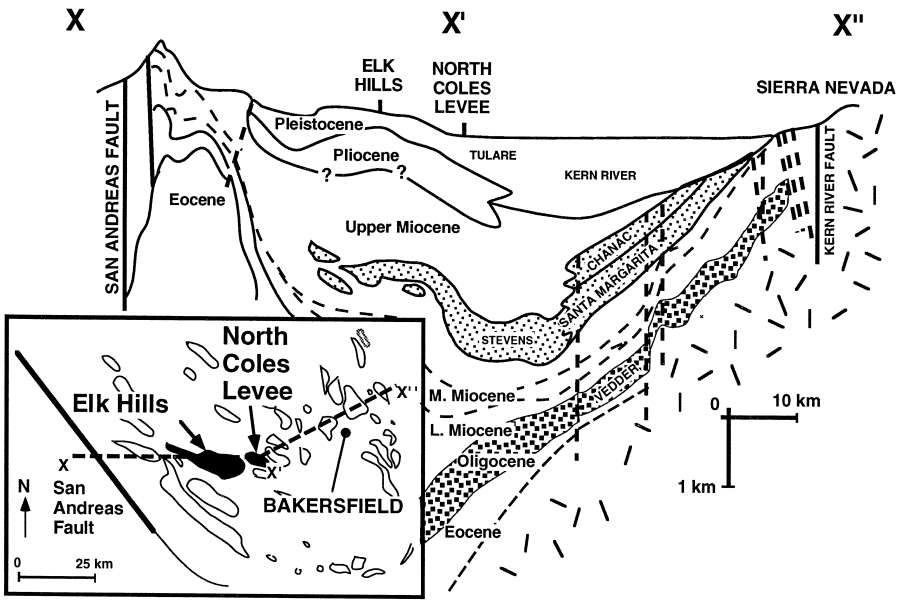

AGE	DEPTH	FM	MEMBER OR ZONE	SAMPLE LOCATIONS
PLEISTOCENE		TULARE FM		
		SAN JOAQUIN		
PLIOCENE	1 km	ETCHEGOIN	SHALLOW OIL ZONE	
		REEF RIDGE SHALE		
	2 km	MONTEREY	ELK HILLS SHALE	EH-3G-B-6a,7a,8 (2.2 km in the Elk Hills Shale of well 352X-3G)
MIOCENE		TEMBLOR FORMATION	MEDIA SHALE	
			CARNEROS SS	
	3 km		U. SANTOS	All samples below are from well 934-29R (Total Depth = 7,445 m)
			AGUA SS	
			LOWER SANTOS SHALE	
	4 km		WYGAL SANDSTONE	EH-29R-A-4 (4.1 km; 153°C)
OLIGOCENE			SALT CREEK	
	5 km		OCEANIC SANDSTONE	EH-29R-A-2 and A-3 (5.3 km; 170°C)
			TUMEY SHALE	
	6 km		KREYENHAGEN SHALE	EH-29R-A-1 (6.1 km; 200°C)
EOCENE			POINT OF ROCKS	
	7 km		CANOAS SILTSTONE	
UPPER CRET.			UNDIFF.	

Fig. 2. Cross section across the Bakersfield arch in the southern San Joaquin basin Elk Hills. Modified from Hayes and Boles (1993). The stratigraphy of the Elk Hills oil field is shown on the right. Modified from Reid (1990a).

the east of the reserve, the 31S anticline bifurcates into north and south segments that form the anticlines defining the structure at the Coles Levee oil fields (Maher et al., 1975).

Several deep wells were drilled within NPR-1 in an attempt to assess the petroleum potential below the Miocene Monterey formation and to assess the structural development of deeper levels (Figs. 1 and 2). The deepest of these wells (934-29R) was drilled to a depth of 7445 m through the crest of the 29R anticline and bottomed in Cretaceous sediments (Fishburn, 1990; McJanet, 1993). As a result, a stratigraphic section of over 7 km has been documented (Fig. 2; Reid, 1990a). Four core segments of Eocene to Oligocene arkosic sandstones from well 934-29R were obtained (Appendix A). Static temperature measurements for these four samples vary from 150° to 200°C (Fishburn, 1990; Appendix A), placing them in the range corresponding to partial degassing of argon from K-feldspar.

Assignment of depositional ages in the deep exploratory wells at Elk Hills is in general based on foraminifera in the Tertiary portion of the section and calcareous nanoplankton in the Cretaceous rocks (Fishburn, 1990). Turbidites of the Monterey formation are comprised mostly of organic-rich diatomite, shales, and sandstone (Reid, 1990b). The Stevens turbidites are thought to have been derived primarily from denudation of the Sierra Nevada batholith (MacPherson, 1977; Milliken et al., 1993; Wilson and McJanet, 1993) with deposition occurring in the upper Mohnian (i.e., 6 to 10 Ma; Calloway, 1990). The typical cement in the Stevens sandstone in the southern San Joaquin basin is calcium carbonate with lesser amounts of quartz and clays (Wood and Boles, 1991; Reid, 1990b; Tieh et al., 1986).

3. $^{40}Ar/^{39}Ar$ analytical methods and approach

3.1. Background

Two kinds of information regarding argon retentivity of K-feldspars are available from an $^{40}Ar/^{39}Ar$ step-heating experiment: the age spectrum, reflecting ^{40}Ar loss in nature, and the Arrhenius plot, representing ^{39}Ar loss in the laboratory. Model ages are calculated from the flux ratio of radiogenic argon ($^{40}Ar*$) to the reactor produced ^{39}Ar evolved during laboratory step-heating. Because ^{39}Ar is essentially uniformly distributed within K-feldspars, the internal distribution of the daughter product can be inferred from step-heating results. The associated Arrhenius diagram, derived by plotting model diffusion coefficients against the inverse temperature of laboratory heating, is a convolution of the parameters that characterize the individual diffusion domains (whether these be dictated by varying length scale, energies, etc.). The multi-diffusion domain (MDD) model (Lovera et al., 1989, 1991, 1997) assumes that the form of the Arrhenius plot and age spectrum are a function of the diffusion parameters for each discrete size domain (activation energy, E, and frequency factor, D_o/r_o^2), and the domain distribution parameters (domain size, ρ, and volume fraction, ϕ). In addition, the age spectrum is also a function of the thermal history. This model has been widely used to recover thermal histories from slowly cooled rocks, but can be adapted to constrain thermal histories of samples that experienced argon loss due to reheating (Quidelleur et al., 1997), such as that expected in a sedimentary basin environment.

Traditionally, K-feldspar $^{40}Ar/^{39}Ar$ thermal history analysis using the MDD model approach has been applied to either individual crystals (Lovera et al., 1991) or polycrystalline samples (e.g., Quidelleur et al., 1997) in which, barring recrystallization effects, all constituent grains from a given rock share the same history. Consequently, it may not be obvious how the technique could be applied to clastic rocks where individual grains are derived from diverse source regions with widely different thermal histories. However, polygenetic feldspar grains from deeply buried sandstone sample share a common thermal overprint imparted during burial, and it is recovering this common history that we target. Although the potentially diverse ^{40}Ar retention properties of a mixed provenance K-feldspar aggregate might appear to represent a limitation in the interpretation of the $^{40}Ar/^{39}Ar$ results in terms of thermal history, we emphasize that this is not the case. Provided that all the grains share a common re-heating history in the basin, an adequate description of their bulk argon diffusion properties is all that is required to recover the thermal history information from the affected portion of the age spectrum. As

formulated, the MDD model is uniquely suited to this task. Indeed, a statistical appraisal of the diffusion parameters and domain distribution characteristics of a wide suite of basement K-feldspar samples (Lovera et al., 1997) has revealed broad similarities in activation energy, frequency factor, and domain distribution. This congruence in argon retention properties causes polygenetic detrital aggregates to exhibit ^{39}Ar release systematics that closely resemble, and can be interpreted in a similar manner to, those of K-feldspars sampled from basement outcrops (Harrison and Bé, 1983; Heizler and Harrison, 1991).

3.2. Removal of Cl-correlated excess ^{40}Ar

Earlier $^{40}Ar/^{39}Ar$ studies of detrital K-feldspars from the San Joaquin basin (Harrison and Bé, 1983; Harrison and Burke, 1988) documented a high degree of contamination by $^{40}Ar_E$. This contamination is responsible for the anomalously old ages observed in the low temperature steps, which limit assessment of the thermal history content of the $^{40}Ar/^{39}Ar$ data. The $^{40}Ar_E$ contamination of in situ radiogenic $^{40}Ar(^{40}Ar_R)$ at low-temperatures is due to decrepitation of fluid inclusions (Harrison et al., 1993). A recently developed method takes advantage of the correlated release of both $^{38}Ar_{Cl}$ (produced as a consequence of a neutron reaction on ^{37}Cl) and $^{40}Ar_E$, as revealed by contiguous isothermal heating steps (Harrison et al., 1994) and provides the basis for correcting measured $^{40}Ar/^{39}Ar$ ratios for $^{40}Ar_E$. Specifically, the first isothermal step is interpreted to yield an anomalously old age and elevated Cl/K ratio due to evolution of $^{40}Ar_E$ and Cl-derived $^{38}Ar(^{38}Ar_{Cl})$ from saline fluid liberated during decrepitation of fluid inclusions. Since the number of fluid inclusions that burst at a given temperature decreases with progressive heating, the second and successive steps are substantially less affected and thus, yield younger ages (see Tables 2–5). Differences in age (i.e., $(^{40}Ar*/K)$) and Cl/K between successive temperature pairs commonly yield a well-correlated array that identifies the Cl-correlated $^{40}Ar_E$ affecting that sample (Harrison et al., 1994). The slope of this array $(^{40}Ar_E/Cl)$ is then used in conjunction with the measured Cl/K ratio of each heating step to remove the effect of the contaminating Cl-correlated $^{40}Ar_E$.

From the above discussion it is clear that for the correction we apply to be meaningful, fluid-inclusion hosted $^{40}Ar_E$ must be characterized by a constant $^{40}Ar_E/Cl$. While this may seem unlikely for polygenetic grains, we point out that basin-derived fluids are also trapped in inclusions within the feldspars during burial diagenesis. To the extent that these fluids represent the principal source of $^{40}Ar_E$, we expect a constant, low value of $^{40}Ar_E/Cl$ during furnace degassing typical of those obtained from young basinal fluids ($\sim 10^{-5}$; Harrison et al., 1994). However, we emphasize that even if $^{40}Ar_E$ is not dominated by basinal fluids, near constant values of $^{40}Ar_E/Cl$ are still anticipated due to homogenization produced by the decrepitation process in which new, smaller inclusions form along failure planes (Harrison et al., 1993, 1994). Therefore, even though it is possible that the $^{40}Ar_E/Cl$ values obtained may not possess geological significance, their utility in correcting for $^{40}Ar_E$ is undiminished since they describe the fluid homogenized during laboratory heating that contributes $^{40}Ar_E$.

3.3. Sample preparation and analysis

K-feldspar is generally abundant in sands derived from deeply dissected arcs (Dickinson, 1974) and, unlike plagioclase, is highly resistant to alteration during diagenesis. Four arkosic sandstones sampled in cores obtained at depths between 4.12 to 6.61 km in well 934-29R were selected for $^{40}Ar/^{39}Ar$ analysis (Appendix A). To obtain the coarsest grain size possible (40–60 mesh), the samples were crushed and sized between 40 to 60 mesh after ultrasonic treatment with 5% H_3PO_4 for 3 h to dissolve carbonate cement. A K-feldspar concentrate was obtained using heavy liquids and a magnetic separator, and the final separate was hand-purified. All separates were high purity (> 99%) alkali feldspar concentrates that contained both clear and cloudy grains. Although sample A1 (EH-29R-A-1) was texturally uniform, A2 (EH-29R-A-2) contained appreciable composite and/or highly recrystallized grains with some very small particles present. Both A1 and A2 yielded 11% equivalent K_2O (see Tables 2 and 3), indicating the presence of minor albite and/or inter-

grown quartz. Sample A3 (EH-29R-A-3) yielded higher equivalent K_2O (15.4%; Table 4) but also contained a significant population of fine grain sizes. Sample A4 (EH-29R-A-4) gave a low equivalent K_2O yield (5%; Table 5) that indicated a large proportion of the alkali feldspar concentrated was albitic. A large number of polycrystalline grains present in A4 were removed by handpicking prior to analysis.

Separate splits from each sample were prepared for both laser and furnace step-heating. The samples were weighed, wrapped in Al or Sn foil, and sealed in 7 mm OD quartz tubes together with regularly distributed Fish Canyon sanidine flux monitors (27.8 $\pm$ 0.3 Ma; Cebula et al., 1986). The assembly was irradiated for 45 h in the L-67 position of the Ford Reactor, University of Michigan. Calculated J factors varied from 0.006577 to 0.006601. Samples wrapped in Sn foil were step-heated in a resistance furnace and those packaged in Al foil were analyzed by laser fusion. All isotopic measurements were undertaken using a VG3600 rare gas mass spectrometer. $^{40}Ar/^{39}Ar$ analytical methods followed those described by Quidelleur et al. (1997). Typical extraction line backgrounds for m/e 36, 39, and 40 were 4×10^{-18} mol, 1×10^{-18} mol, and 4×10^{-16} mol, respectively. $^{40}Ar/^{36}Ar$ ratios measured for atmospheric argon during the course of these analyses averaged 301.0 ± 2.5 (1σ). Correction factors for nucleogenic argon determined from K_2SO_4 and CaF_2 salts were as follows: $(^{40}Ar/^{39}Ar)_K = 2.5 \pm 0.1 \times 10^{-2}$; $(^{38}Ar/^{39}Ar)_K = 1.20 \pm 0.01 \times 10^{-2}$; $(^{36}Ar/^{37}Ar)_{Ca} = 2.5 \pm 0.2 \times 10^{-4}$; $(^{39}Ar/^{37}Ar)_{Ca} = 7.0 \pm 0.7 \times 10^{-4}$. Production ratios used to calculate Cl and Ca relative to K were determined from previous irradiations: $Cl/K = 0.277 \cdot (^{38}Ar_{Cl}/^{39}Ar_K)$ and $Ca/K = 2.02 \cdot (^{37}Ar_{Ca}/^{39}Ar_K)$. Data summaries are provided in Tables 2–5 while results are shown in Figs. 3–7. Complete data tables may be obtained from http://oro.ess.ucla.edu/argon/elk.html.

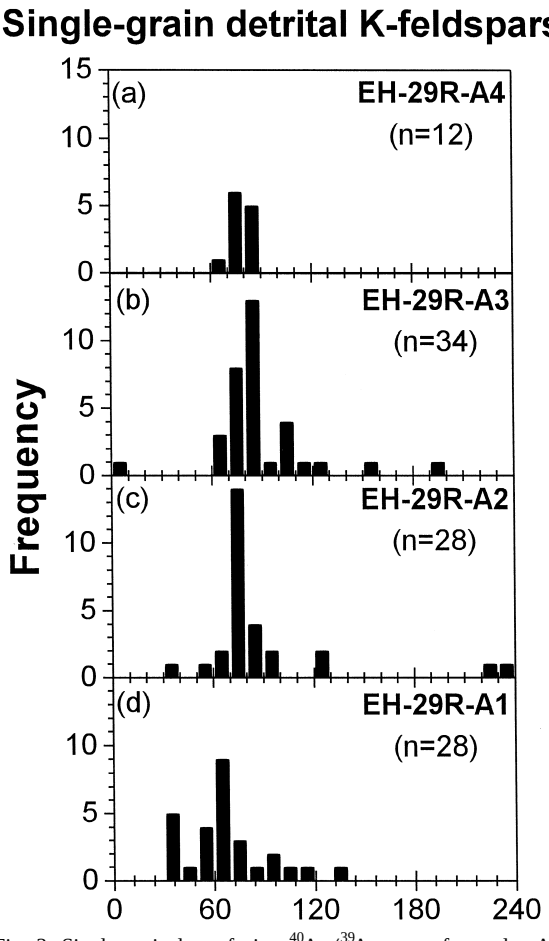

Fig. 3. Single grain laser fusion $^{40}Ar/^{39}Ar$ ages of samples A1, A2, A3, and A4 from NPR-1 well 934-29R.

4. Results

4.1. Single-crystal laser fusion

Individual single detrital K-feldspar grains were fused using an Ar-ion laser and dated by the $^{40}Ar/^{39}Ar$ method in order to obtain broad insights into the age distribution of each of these samples. The results of these analyses are shown in histogram form in Fig. 3. All four samples yield a range of apparent ages that are broadly consistent with those measured for basement outcrops in the Sierra Nevada (i.e., mostly Cretaceous with some Jurassic and Triassic granitoids; Barton et al., 1988) and the Salinian block (Upper Cretaceous granitoids; Mattinson, 1978). There is a general trend for grains extracted from the deeper samples to yield younger ages than shallower samples. While this is opposite the trend expected from sediment originating from a progressively denuding mountain range, it is the behavior anticipated for detrital K-feldspars that have experienced increasing $^{40}Ar*$ loss with depth. Such an

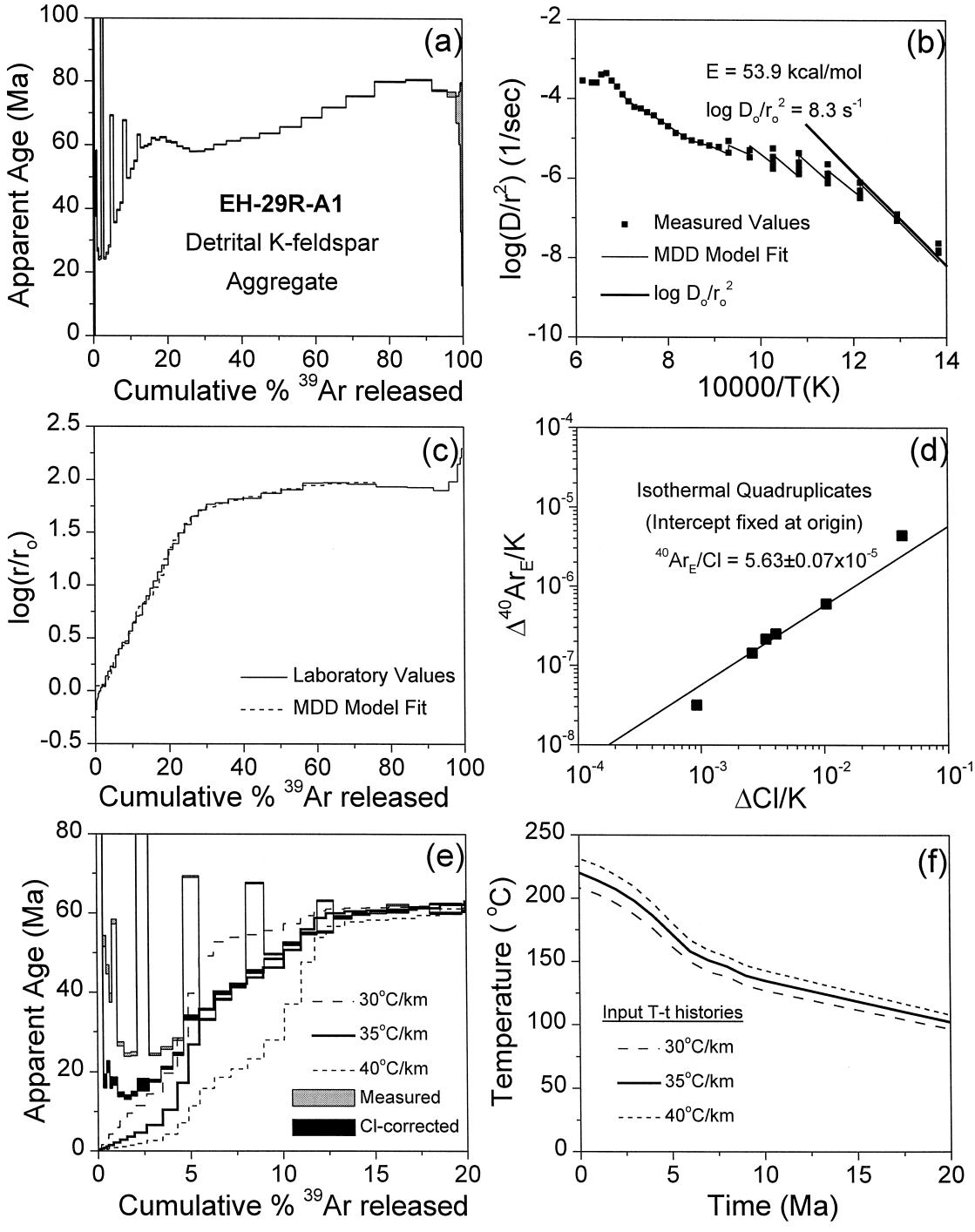

Fig. 4. Sample EH-29R-A-1 (a) age spectrum, (b) Arrhenius plot, (c) log (r/r_0) plot, (d) log $\Delta(^{40}\mathrm{Ar}*/\mathrm{K})$ vs. log $\Delta(\mathrm{Cl}/\mathrm{K})$ plot, (e) Cl-corrected age spectrum with model age spectra, and (f) thermal history.

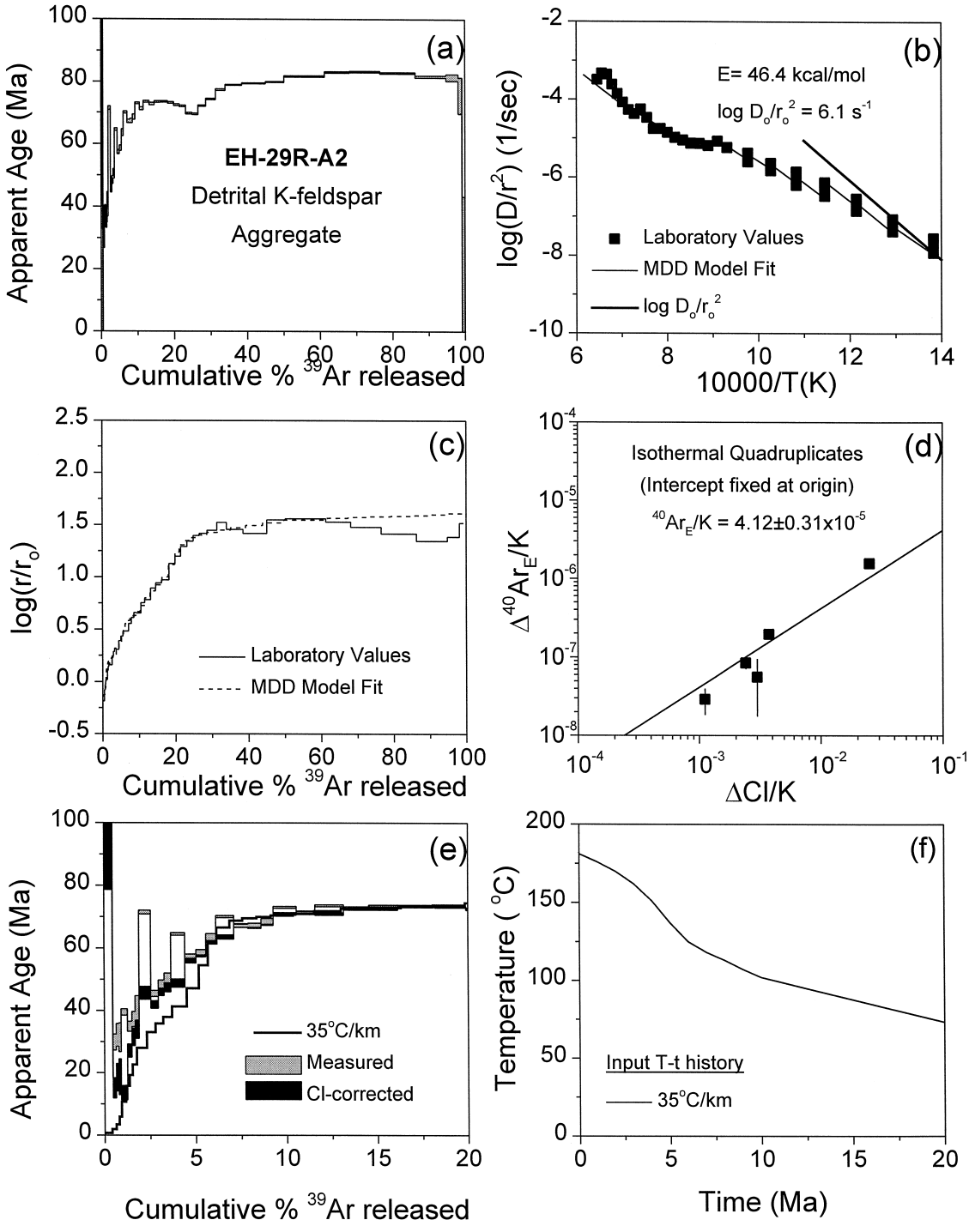

Fig. 5. Sample EH-29R-A-2 (a) age spectrum, (b) Arrhenius plot, (c) log (r/r_0) plot, (d) log $\Delta(^{40}\mathrm{Ar}*/\mathrm{K})$ vs. log $\Delta(\mathrm{Cl}/\mathrm{K})$ plot, (e) Cl-corrected age spectrum with model age spectra, and (f) thermal history.

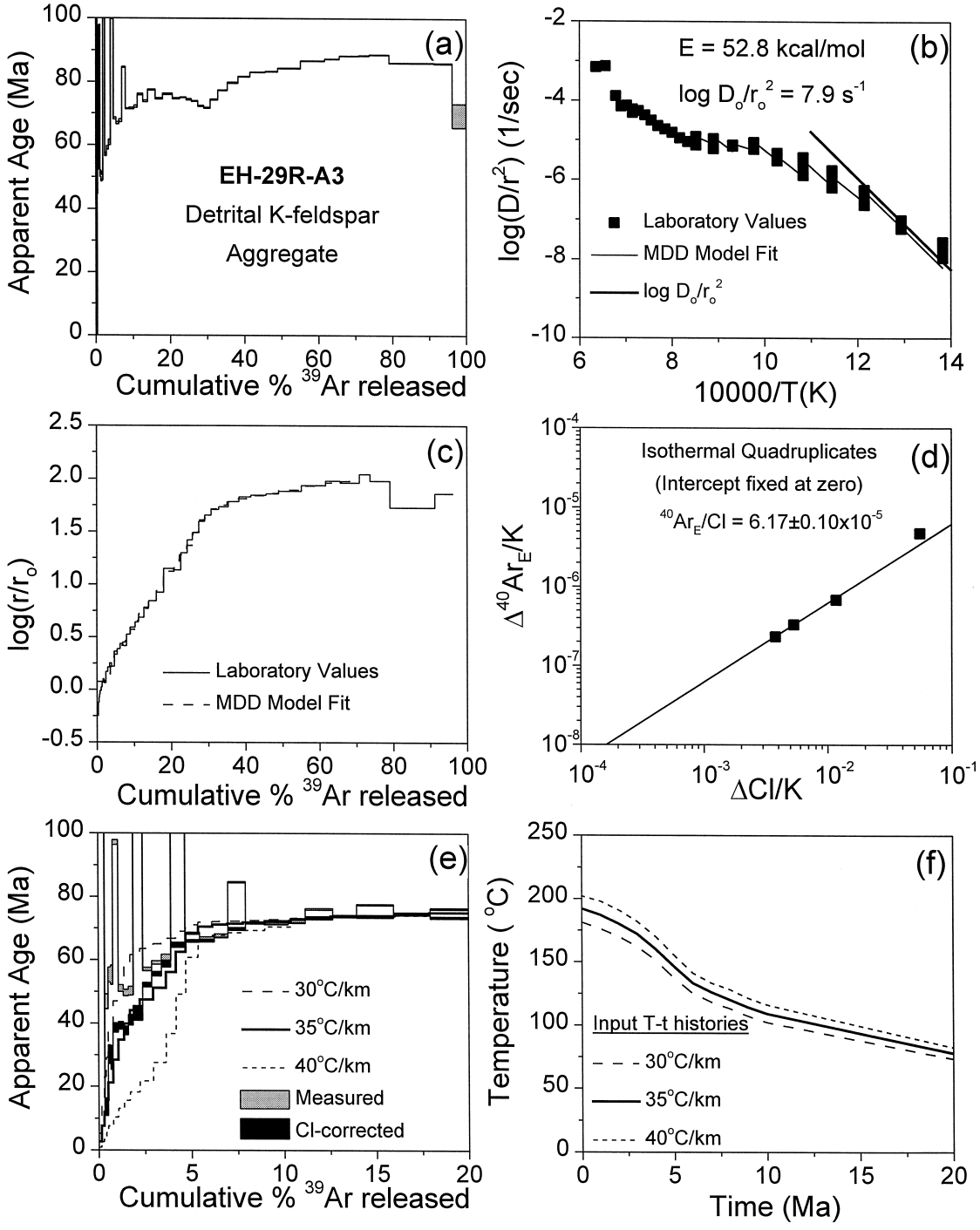

Fig. 6. Sample EH-29R-A-3 (a) age spectrum, (b) Arrhenius plot, (c) log (r/r_0) plot, (d) log $\Delta(^{40}\mathrm{Ar}*/\mathrm{K})$ vs. log $\Delta(\mathrm{Cl}/\mathrm{K})$ plot, (e) Cl-corrected age spectrum with model age spectra, and (f) thermal history. Candidate thermal histories for A3 using three possible geothermal gradients. Computed from one-dimensional conductive heat flow model using Eq. (2).

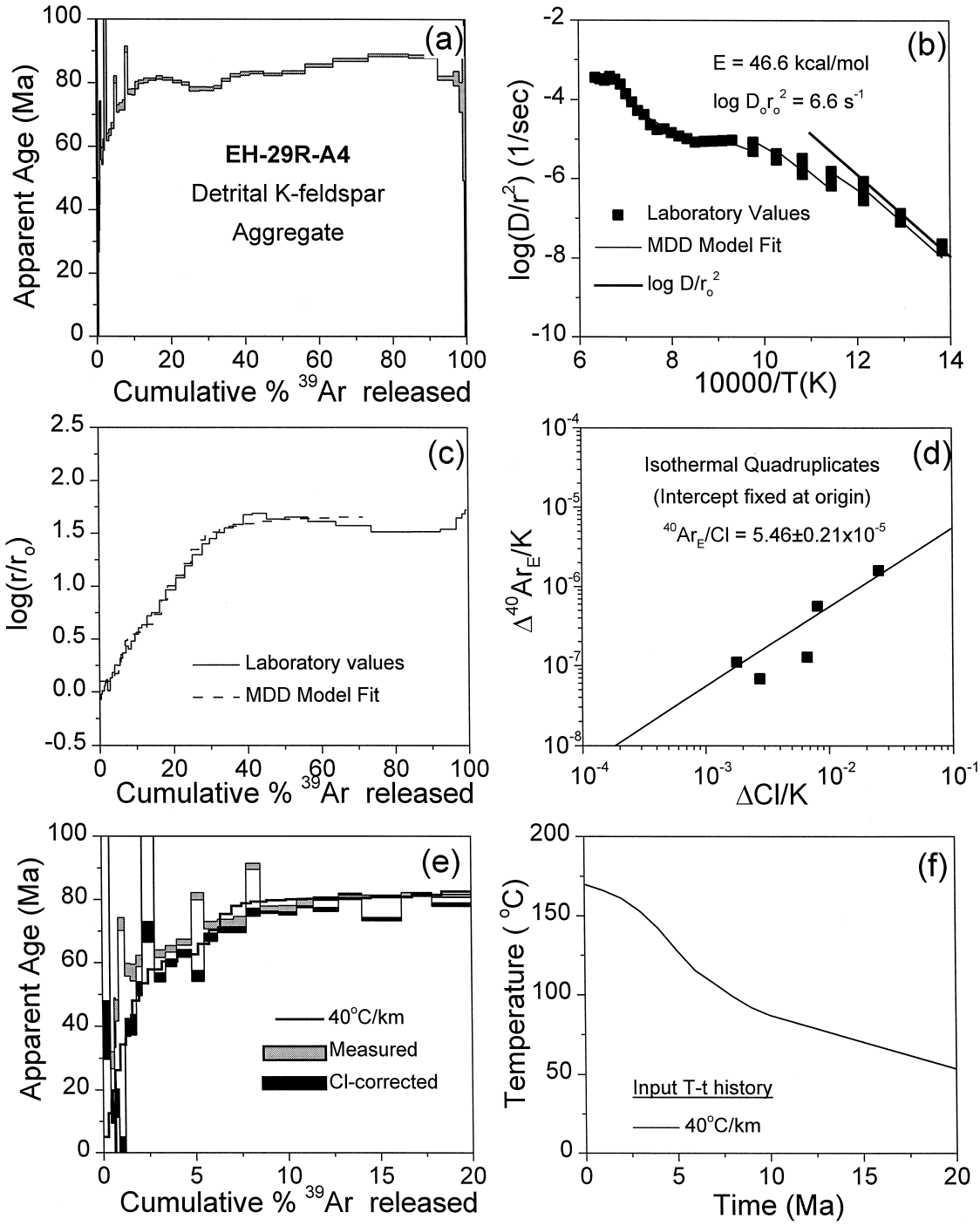

Fig. 7. Sample EH-29R-A-4 (a) age spectrum, (b) Arrhenius plot, (c) log (r/r_0) plot, (d) log $\Delta(^{40}\mathrm{Ar}*/\mathrm{K})$ vs. log $\Delta(\mathrm{Cl}/\mathrm{K})$ plot, (e) Cl-corrected age spectrum with model age spectra, and (f) thermal history.

interpretation is also implied by the fact that several grains from the deepest sample (A1) yield dates that are younger than the ca. 45 Ma depositional age.

4.2. Step-heating experiments

Each of the four detrital K-feldspar aggregates was analyzed by the $^{40}Ar/^{39}Ar$ step-heating method using a resistance furnace. In order to improve the basis for correcting the low-temperature argon release from these feldspars and improve the resolution of the kinetic parameters, isothermal quadruplicates were obtained for the first five temperature steps, 450°, 500°, 550°, 600°, and 650°C, using heating times of 5, 10, 15, and 20 min respectively. After this treatment, temperature was increased monotonically until gas extraction was complete. Measured age spectra for the respective samples are displayed in Fig. 4a, Fig. 5a, Fig. 6a, Fig. 7a and Fig. 4b, Fig. 5b, Fig. 6b and Fig. 7b show the Arrhenius plots (log D/r^2 vs. $1/T$) calculated for all four samples.

4.2.1. Determination of diffusion parameters and domain distributions

The diffusion parameters E and $\log(D/r_o^2)$ characterizing our samples are necessarily average values determined by the relative contributions of individual grains that are each characterized by their own intrinsic diffusion parameters. Based upon examination of numerous individual basement K-feldspar samples analyzed by Lovera et al. (1997), we expect our detrital samples to yield $E = 47 \pm 6$ kcal/mol and $\log(D/r_o^2) = 4.8 \pm 1.5$ s^{-1}. According to the MDD model, the initial array of $\log(D/r^2)$ values obtained from single-E specimens are anticipated to form a linear array proportional to activation energy as long as the gas fractions released from the smallest domains do not exceed $\sim 60\%$ (Lovera et al., 1997). For each of the detrital aggregates we examined, there is a detectable decrease in $\log(D/r^2)$ during isothermal heating. This drop signals the existence of very small, though volumetrically important domains (Lovera et al., 1997). Thorough outgassing of these unretentive domains during low-temperature heating affects the measured $\log(D/r^2)$ values in such a manner that the slope of the initial array of Arrhenius data may significantly underestimate E (Lovera et al., 1997). In order to counteract this effect, the diffusion parameters were determined using the average maximum slope obtained from the last step and first step of the first three adjoining isothermal quadruplicates. This technique yields values of E and $\log(D/r_o^2)$ that better approximate the true diffusion parameters in unretentive samples (Lovera et al., 1997).

Limitations in conventional Arrhenius plots for step-heating data for samples containing multiple diffusion domains are overcome by use of the $\log(r/r_o)$ spectrum-type plot (Richter et al., 1991). Fig. 4c, Fig. 5c, Fig. 6c and Fig. 7c are plots of $\log(r/r_o)$ vs. cumulative % ^{39}Ar released. Once E and D_o/r_o^2 were determined, we calculated sets of domain distribution parameters using an automated routine that systematically varies size (ρ) and volume fraction (ϕ) of domains until the best fit to the $\log(r/r_o)$ plot is obtained (Quidelleur et al., 1997). Quite often the age spectra and $\log(r/r_o)$ plots yielded by K-feldspars contain correlated inflections that indicate the presence of a discrete distribution of argon retentivities in the samples. The $\log(r/r_o)$ plots yielded by our samples increase smoothly with increasing ^{39}Ar release, indicating an effectively continuous distribution of domains that is consistent with the nature of the detrital material examined. Accordingly we have modeled all samples with 10 domains, a number that effectively yields a continuous distribution.

The MDD model fits determined for the Arrhenius and $\log(r/r_o)$ plots are shown in Fig. 4b, Fig. 5b, Fig. 6b, Fig. 7b and Fig. 4c, Fig. 5c, Fig. 6c and Fig. 7c, respectively. Fits using the automated routine tend to underestimate the diffusivity of the earliest gas released for all samples. Because the effect for sample A2 was significant, manual adjustment of the fitting was performed in order to achieve a relatively good match to the laboratory models. The distribution and Arrhenius parameters for all four samples are given in Table 1.

4.2.2. Correction of age spectra for Cl-correlated $^{40}Ar_E$

Age spectra uncorrected for Cl-correlated $^{40}Ar_E$ are characterized by highly variable ages reflecting the presence of $^{40}Ar_E$, thus are of little use in constraining the thermal history of the basin. However, correction for Cl-correlated $^{40}Ar_E$ has the potential to

Table 1
Arrhenius and domain distribution parameters

	EH-29R-A-1 (E = 53.9 kcal/mol)		EH-29R-A-2 (E = 46.4 kcal/mol)		EH-29R-A-3 (E = 52.8 kcal/mol)		EH-29R-A-4 (E = 47.6 kcal/mol)	
	volume fraction (ϕ)	$\log(D_o/r^2)$ (s^{-1})	volume fraction (ϕ)	$\log(D_o/r^2)$ (s^{-1})	volume fraction (ϕ)	$\log(D_o/r^2)$ (s^{-1})	volume fraction (ϕ)	$\log(D_o/r^2)$ (s^{-1})
1	0.0306	10.88	0.0052	10.52	0.0259	10.54	0.0426	8.87
2	0.0515	9.53	0.0300	8.22	0.0460	9.09	0.0967	7.03
3	0.0808	8.17	0.0040	6.84	0.0753	7.97	0.0320	6.09
4	0.0362	7.06	0.0379	6.84	0.0845	6.83	0.0397	5.87
5	0.1021	5.36	0.0808	5.90	0.0706	4.86	0.2058	3.33
6	0.0694	4.54	0.0541	3.87	0.0890	4.56	0.2295	3.30
7	0.2139	4.34	0.1954	3.20	0.1461	3.97	0.1525	3.30
8	0.2462	4.34	0.4637	2.92	0.1983	3.94	0.1138	3.28
9	0.1679	4.31	0.1288	2.79	0.2376	3.87	0.0876	3.26
10	0.0013	2.30	0.0001	0.10	0.0268	1.90	0.0001	0.60

Table 2
$^{40}Ar/^{39}Ar$ results for EH-29R-A1 K-feldspar (27.26 mg; $J = 0.006577$)

Step	T (C)	t (min)	$^{40}Ar/^{39}Ar$	$^{8}Ar/^{39}Ar$ $\times 10^{-3}$	$^{37}Ar/^{39}Ar$ $\times 10^{-4}$	$^{36}Ar/^{39}Ar$ $\times 10^{-3}$	moles ^{39}Ar $\times 10^{-14}$	% ^{39}Ar released	% $^{40}Ar*$	Cl/K^{a} $\times 10^{-4}$	$^{40}Ar*/^{39}Ar_{K}$ $\times 10^{-1}$	Conventional age (Ma)	Cl-corrected Age[b] (Ma)
1	450	5	83.31	198.1	105.6	80.41	1.561	0.2987	71.45	474 ± 6	595.3 ± 3.4	596.0 ± 2.4	289.0 ± 6.7
2	450	11	25.05	40.91	70.79	69.38	0.8999	0.4709	18.06	44.0 ± 1.1	45.25 ± 1.25	52.90 ± 1.40	17.67 ± 1.78
3	450	17	11.39	27.85	58.20	25.23	0.8817	0.6396	34.32	30.8 ± 1.2	39.09 ± 1.01	45.80 ± 1.15	21.30 ± 1.53
4	450	20	6.177	23.49	54.53	9.691	0.7618	0.7854	53.25	26.8 ± 1.1	32.89 ± 0.98	38.61 ± 1.14	17.29 ± 1.47
5	500	5	6.478	31.02	55.06	5.092	1.394	1.052	76.39	50.0 ± 0.9	49.49 ± 0.52	57.79 ± 0.59	17.67 ± 1.06
6	500	10	3.419	18.52	45.34	3.734	1.888	1.414	67.01	16.1 ± 0.4	22.91 ± 0.44	26.98 ± 0.51	14.33 ± 0.61
7	500	15	3.100	17.59	48.16	3.432	1.893	1.776	66.49	13.7 ± 0.4	20.61 ± 0.37	24.29 ± 0.43	13.62 ± 0.56
8	500	20	3.189	17.36	40.59	3.659	1.792	2.119	65.32	12.9 ± 0.4	20.83 ± 0.40	24.55 ± 0.47	14.51 ± 0.60
9	550	5	10.70	53.82	58.92	4.641	3.323	2.755	86.96	113 ± 1	93.06 ± 0.30	107.2 ± 0.3	16.73 ± 1.60
10	550	10	2.544	15.46	53.67	1.526	3.335	3.393	81.31	8.80 ± 0.25	20.69 ± 0.24	24.38 ± 0.29	17.74 ± 0.35
11	550	15	2.777	14.78	50.53	1.860	3.359	4.036	79.33	6.73 ± 0.24	22.03 ± 0.27	25.96 ± 0.31	21.02 ± 0.37
12	550	20	3.023	14.25	50.72	2.050	3.065	4.622	79.15	5.17 ± 0.28	23.93 ± 0.28	28.17 ± 0.32	24.52 ± 0.38
13	600	5	6.845	28.73	66.05	2.959	4.596	5.502	86.87	44.8 ± 0.6	59.46 ± 0.19	69.21 ± 0.21	33.63 ± 0.66
14	600	10	3.296	13.53	55.18	0.7991	4.573	6.377	92.09	3.83 ± 0.20	30.36 ± 0.16	35.66 ± 0.19	33.12 ± 0.23
15	600	15	3.645	12.99	50.34	0.8450	4.496	7.237	92.47	2.31 ± 0.22	33.71 ± 0.16	39.56 ± 0.19	38.26 ± 0.23
16	600	20	3.925	12.70	49.10	1.113	4.085	8.019	90.99	1.36 ± 0.23	35.71 ± 0.18	41.89 ± 0.21	41.35 ± 0.23
17	650	5	6.463	22.68	68.43	2.134	5.160	9.007	89.86	28.5 ± 0.4	58.08 ± 0.17	67.63 ± 0.19	45.29 ± 0.46
18	650	10	4.455	12.91	57.93	0.6223	5.362	10.03	95.32	2.19 ± 0.18	42.46 ± 0.14	49.69 ± 0.16	48.49 ± 0.19
19	650	15	4.742	12.63	51.50	0.7557	5.116	11.01	94.77	1.35 ± 0.16	44.94 ± 0.16	52.55 ± 0.18	52.03 ± 0.19
20	650	20	4.988	12.53	49.57	0.8575	4.617	11.90	94.43	1.02 ± 0.22	47.10 ± 0.17	55.03 ± 0.20	54.79 ± 0.21
21	700	5	5.744	16.00	60.53	1.029	4.638	12.78	94.28	10.6 ± 0.2	54.15 ± 0.16	63.14 ± 0.18	55.23 ± 0.27
22	700	10	5.267	12.57	50.62	0.5808	5.287	13.80	96.27	1.29 ± 0.23	50.71 ± 0.15	59.18 ± 0.16	58.72 ± 0.19
23	700	15	5.357	12.33	45.76	0.7478	5.186	14.79	95.41	0.51 ± 0.20	51.12 ± 0.16	59.65 ± 0.18	59.81 ± 0.20
24	700	20	5.485	12.47	44.63	1.021	4.671	15.68	94.05	0.77 ± 0.20	51.58 ± 0.18	60.19 ± 0.20	60.14 ± 0.20

25	750	10	5.662	13.24	52.13	1.061	6.272	16.88	94.03	2.88 ± 0.22	53.24 ± 0.20	62.09 ± 0.22	60.35 ± 0.26
26	750	15	5.531	12.45	46.19	0.7707	5.886	18.01	95.44	0.85 ± 0.14	52.79 ± 0.15	61.57 ± 0.16	61.46 ± 0.17
27	800	10	5.669	13.49	55.00	0.9944	9.223	19.77	94.38	3.61 ± 0.16	53.50 ± 0.16	62.39 ± 0.17	60.06 ± 0.21
28	800	15	5.531	12.66	51.06	0.9047	6.563	21.03	94.72	1.37 ± 0.20	52.39 ± 0.22	61.12 ± 0.25	60.59 ± 0.27
29	825	15	5.552	12.95	55.37	1.082	8.391	22.64	93.80	2.06 ± 0.64	52.08 ± 0.19	60.76 ± 0.18	–
30	850	15	5.485	12.93	58.30	1.201	8.484	24.26	93.08	1.96 ± 0.55	51.06 ± 0.14	59.59 ± 0.14	–
31	875	15	5.439	13.41	62.09	1.232	9.328	26.04	92.86	3.26 ± 0.59	50.51 ± 0.13	58.95 ± 0.15	–
32	900	15	5.414	14.17	59.74	1.421	9.928	27.94	91.79	5.26 ± 0.63	49.69 ± 0.11	58.02 ± 0.12	–
33	925	15	5.438	15.22	59.89	1.476	11.28	30.10	91.52	8.14 ± 0.64	49.77 ± 0.12	58.11 ± 0.12	–
34	950	15	5.458	16.47	58.24	1.380	12.96	32.58	92.08	11.7 ± 0.7	50.26 ± 0.12	58.67 ± 0.13	–
35	975	15	5.553	17.43	59.93	1.270	17.50	35.93	92.80	14.4 ± 0.8	51.53 ± 0.08	60.13 ± 0.09	–
36	1000	15	5.633	17.77	63.16	1.194	20.39	39.83	93.30	15.4 ± 0.8	52.55 ± 0.08	61.30 ± 0.09	–
37	1025	15	5.703	17.91	69.11	1.173	26.66	44.94	93.49	15.8 ± 0.8	53.31 ± 0.09	62.18 ± 0.09	–
38	1050	15	5.809	18.05	78.01	1.111	28.73	50.43	93.93	16.2 ± 0.8	54.56 ± 0.08	63.60 ± 0.08	–
39	1075	15	6.024	18.51	92.47	1.235	30.61	56.29	93.54	17.4 ± 0.8	56.34 ± 0.07	65.65 ± 0.07	–
40	1100	15	6.332	19.42	105.1	1.409	28.94	61.83	93.04	19.8 ± 0.8	58.91 ± 0.08	68.58 ± 0.08	–
41	1125	15	6.659	20.76	100.8	1.561	34.24	68.38	92.71	23.5 ± 0.9	61.73 ± 0.10	71.80 ± 0.10	–
42	1150	15	6.999	20.89	80.67	1.652	40.58	76.15	92.67	23.8 ± 1.0	64.86 ± 0.09	75.36 ± 0.10	–
43	1175	15	7.485	19.20	49.09	1.936	44.30	84.63	92.03	18.9 ± 0.8	68.88 ± 0.13	79.93 ± 0.13	–
44	1200	15	7.909	17.13	22.37	3.196	37.28	91.76	87.75	12.6 ± 0.8	69.40 ± 0.15	80.52 ± 0.16	–
45	1225	11	8.118	16.04	18.06	4.885	21.68	95.91	81.91	8.64 ± 0.71	66.50 ± 0.22	77.23 ± 0.25	–
46	1250	15	11.28	17.84	30.98	15.96	12.46	98.30	57.98	7.87 ± 0.82	65.42 ± 0.68	76.01 ± 0.77	–
47	1275	15	31.25	31.68	42.16	84.92	3.758	99.02	19.62	10.3 ± 1.5	61.30 ± 3.85	71.31 ± 4.29	–
48	1300	15	50.70	46.52	53.19	151.5	2.171	99.43	11.62	16.7 ± 2.7	58.92 ± 7.68	68.59 ± 8.31	–
49	1350	15	121.1	93.44	89.46	393.3	1.383	99.70	3.984	20.9 ± 5.5	48.23 ± 22.01	56.34 ± 23.45	–
50	1550	5	137.0	103.4	71.72	449.7	1.592	100	2.960	19.2 ± 6.9	40.55 ± 30.33	47.48 ± 31.50	–

[a] Cl/K offset of 7.1×10^{-5} applied to correct ages.
[b] $^{40}Ar_E/Cl = 5.63 \pm 0.07 \times 10^{-5}$.

Table 3
$^{40}Ar/^{39}Ar$ results for EH-29R-A2 K-feldspar (18.76 mg; $J = 0.006585$)

Step	T (C)	t (min)	$^{40}Ar/^{39}Ar$	$^{8}Ar/^{39}Ar$ $\times 10^{-3}$	$^{37}Ar/^{39}Ar$ $\times 10^{-4}$	$^{36}Ar/^{39}Ar$ $\times 10^{-3}$	moles ^{39}Ar $\times 10^{-14}$	% ^{39}Ar released	% $^{40}Ar*$	Cl/K^{a} $\times 10^{-4}$	$^{40}Ar*/^{39}Ar_K$	Conventional age (Ma)	Cl-corrected Age[b] (Ma)
1	450	10	37.30	121.9	124.3	51.63	16.86	0.4618	59.03	278 ± 3	22.02 ± 0.15	244.3 ± 1.4	90.86 ± 12.16
2	450	15	17.41	30.53	88.71	50.27	6.437	0.6381	14.54	25.2 ± 1.2	2.532 ± 0.250	29.83 ± 2.55	15.10 ± 3.23
3	450	20	5.941	22.48	107.4	10.78	5.319	0.7838	45.99	23.4 ± 1.4	2.733 ± 0.362	32.17 ± 3.59	18.50 ± 4.46
4	450	25	5.385	21.61	110.9	9.117	4.792	0.9150	49.52	21.9 ± 1.6	2.667 ± 0.476	31.41 ± 4.62	18.67 ± 5.75
5	500	11	4.840	28.77	98.24	4.923	12.28	1.251	69.44	43.9 ± 0.8	3.361 ± 0.098	39.49 ± 1.00	13.57 ± 2.30
6	500	15	4.309	17.80	88.12	4.455	8.892	1.495	68.89	13.8 ± 1.2	2.969 ± 0.166	34.93 ± 1.65	27.08 ± 2.13
7	500	15	4.468	16.50	82.21	4.309	6.564	1.675	70.95	10.2 ± 0.9	3.170 ± 0.237	37.28 ± 2.39	31.54 ± 2.85
8	500	25	6.874	17.61	78.66	11.42	8.223	1.900	50.56	9.60 ± 1.84	3.476 ± 0.369	40.82 ± 3.89	35.48 ± 4.44
9	550	13	7.259	28.73	110.1	3.730	23.43	2.542	84.48	44.4 ± 0.7	6.133 ± 0.058	71.42 ± 0.58	45.66 ± 2.08
10	550	15	4.493	14.76	98.56	2.001	14.92	2.950	86.30	6.61 ± 0.46	3.878 ± 0.099	45.49 ± 0.98	41.93 ± 1.21
11	550	16	4.680	13.85	95.99	1.752	11.52	3.266	88.42	4.22 ± 0.48	4.138 ± 0.134	48.50 ± 1.31	46.37 ± 1.58
12	550	24	4.915	14.20	89.94	1.958	13.50	3.636	87.74	5.09 ± 0.52	4.312 ± 0.161	50.52 ± 1.54	47.88 ± 1.89
13	600	11	6.466	22.42	118.9	3.086	28.42	4.414	85.52	27.3 ± 0.5	5.530 ± 0.041	64.53 ± 0.41	48.84 ± 1.30
14	600	15	5.201	13.26	88.42	0.8911	22.42	5.028	94.47	3.02 ± 0.34	4.913 ± 0.067	57.44 ± 0.66	56.03 ± 0.79
15	600	18	5.365	12.71	80.58	1.081	19.69	5.567	93.59	1.41 ± 0.33	5.021 ± 0.087	58.68 ± 0.84	58.22 ± 1.01
16	600	25	5.729	12.58	76.77	0.8689	20.04	6.116	95.09	1.16 ± 0.39	5.448 ± 0.114	63.58 ± 1.08	63.27 ± 1.31
17	650	12	6.576	16.54	94.24	1.824	35.94	7.101	91.43	11.6 ± 0.3	6.013 ± 0.034	70.05 ± 0.34	63.60 ± 0.65
18	650	15	5.934	12.27	65.15	0.5151	28.19	7.873	97.02	0.47 ± 0.36	5.758 ± 0.054	67.14 ± 0.53	67.23 ± 0.62
19	650	20	6.041	12.50	68.77	0.8244	26.41	8.596	95.56	0.97 ± 0.28	5.773 ± 0.071	67.31 ± 0.67	67.11 ± 0.81
20	650	25	6.093	12.47	59.28	0.6398	24.61	9.270	96.49	0.96 ± 0.37	5.879 ± 0.093	68.52 ± 0.89	68.33 ± 1.07
21	700	14	6.594	13.68	68.83	1.013	46.18	10.54	95.09	4.13 ± 0.27	6.270 ± 0.031	72.99 ± 0.30	70.95 ± 0.41
22	700	20	6.378	12.35	65.66	0.7990	37.77	11.57	95.91	0.54 ± 0.23	6.117 ± 0.049	71.24 ± 0.47	71.29 ± 0.56
23	750	12	6.686	14.09	89.40	1.158	57.18	13.14	94.52	5.19 ± 0.21	6.319 ± 0.028	73.55 ± 0.28	70.89 ± 0.40

24	750	20	6.544	12.48	75.89	0.8904	50.89	14.53	95.61	0.87 ± 0.18	6.257 ± 0.045	72.84 ± 0.41	72.70 ± 0.51
25	800	11	6.720	13.10	72.17	1.287	58.22	16.12	93.98	2.39 ± 0.26	6.315 ± 0.027	73.51 ± 0.26	72.48 ± 0.33
26	825	11	6.697	12.71	62.69	1.204	75.11	18.18	94.32	1.34 ± 0.22	6.316 ± 0.020	73.52 ± 0.21	–
27	850	13	6.631	12.67	65.98	1.081	62.06	19.88	94.81	1.31 ± 0.21	6.287 ± 0.026	73.19 ± 0.26	–
28	875	11	6.616	12.88	70.38	1.233	54.77	21.38	94.12	1.80 ± 0.22	6.227 ± 0.028	72.50 ± 0.29	–
29	900	14	6.601	13.21	66.42	1.313	65.34	23.17	93.75	2.68 ± 0.21	6.188 ± 0.026	72.06 ± 0.26	–
30	925	12	6.379	13.93	61.83	1.247	62.17	24.87	93.84	4.71 ± 0.31	5.986 ± 0.027	69.74 ± 0.28	–
31	950	11	6.387	14.70	64.24	1.342	61.62	26.56	93.41	6.79 ± 0.25	5.966 ± 0.024	69.51 ± 0.25	–
32	975	11	6.739	15.48	73.38	1.738	76.80	28.67	92.02	8.72 ± 0.27	6.201 ± 0.021	72.20 ± 0.22	–
33	1000	12	6.973	16.03	81.39	1.887	97.22	31.33	91.65	10.2 ± 0.2	6.390 ± 0.026	74.36 ± 0.24	–
34	1025	13	7.182	15.80	75.72	1.696	96.69	33.98	92.68	9.65 ± 0.31	6.656 ± 0.023	77.39 ± 0.24	–
35	1050	13	7.260	16.23	82.09	1.503	166.1	38.53	93.55	10.9 ± 0.3	6.792 ± 0.015	78.93 ± 0.16	–
36	1075	13	7.248	15.94	88.16	1.302	239.4	45.08	94.35	10.2 ± 0.3	6.839 ± 0.016	79.47 ± 0.18	–
37	1100	15	7.509	16.77	99.89	2.046	184.5	50.14	91.62	12.1 ± 0.7	6.880 ± 0.017	79.94 ± 0.17	–
38	1125	32	7.922	17.20	92.55	2.919	406.1	61.26	88.81	12.9 ± 0.8	7.036 ± 0.023	81.70 ± 0.22	–
39	1150	16	8.311	17.02	64.26	3.824	252.3	68.17	86.11	11.9 ± 0.8	7.157 ± 0.020	83.08 ± 0.21	–
40	1175	15	8.360	16.69	43.77	3.932	306.4	76.56	85.80	11.0 ± 0.7	7.173 ± 0.023	83.26 ± 0.23	–
41	1200	15	8.475	15.40	23.98	4.449	355.4	86.30	84.19	7.11 ± 0.72	7.135 ± 0.022	82.83 ± 0.24	–
42	1225	15	9.052	15.24	17.61	6.752	309.8	94.78	77.68	5.46 ± 0.69	7.032 ± 0.031	81.66 ± 0.34	–
43	1250	15	13.72	18.03	26.03	22.63	123.3	98.16	51.08	4.91 ± 0.79	7.008 ± 0.098	81.39 ± 1.10	–
44	1275	19	41.93	36.50	58.93	119.9	40.07	99.26	15.48	5.48 ± 1.86	6.490 ± 0.516	75.50 ± 5.83	–
45	1350	30	224.2	157.1	290.5	762.0	27.05	99.99	−0.4319	5.34 ± 10.8	−0.97 ± 5.10	–	–

[a] Cl/K offset of 6.3×10^{-5} applied to correct ages.
[b] $^{40}Ar_E$ /Cl = $4.12 \pm 0.31 \times 10^{-5}$.

Table 4
$^{40}Ar/^{39}Ar$ results for EH-29R-A3 K-feldspar (20.63 mg; $J = 0.006592$)

Step	T (C)	t (min)	$^{40}Ar/^{39}Ar$	$^{8}Ar/^{39}Ar$ $\times 10^{-3}$	$^{37}Ar/^{39}Ar$ $\times 10^{-4}$	$^{36}Ar/^{39}Ar$ $\times 10^{-3}$	moles ^{39}Ar $\times 10^{-14}$	% ^{39}Ar released	% $^{40}Ar*$	Cl/K[a] $\times 10^{-4}$	$^{40}Ar*/^{39}Ar_K$	Conventional age (Ma)	Cl-corrected Age[b] (Ma)
1	450	5	82.12	239.2	20.99	665.4	1.770	0.3245	76.03	595 ± 8	62.43 ± 0.33	621.9 ± 2.31	91.2 ± 10.7
2	450	13	30.61	42.56	8.122	899.8	0.9954	0.5070	13.05	37.8 ± 0.8	3.994 ± 0.221	46.88 ± 2.38	13.57 ± 2.75
3	450	19	8.160	24.59	5.664	115.6	0.8337	0.6598	57.85	28.9 ± 1.2	4.721 ± 0.233	55.29 ± 2.33	30.17 ± 2.96
4	450	20	6.324	23.80	6.745	53.67	0.6288	0.7751	74.53	29.9 ± 1.2	4.714 ± 0.310	55.20 ± 3.05	29.14 ± 3.81
5	500	7	9.849	37.20	5.186	48.47	1.566	1.062	85.21	67.3 ± 0.9	8.392 ± 0.071	97.14 ± 0.74	38.68 ± 1.50
6	500	10	5.375	17.62	4.804	33.78	1.458	1.330	80.97	13.8 ± 0.5	4.353 ± 0.099	51.04 ± 1.07	39.30 ± 1.25
7	500	15	5.193	17.68	6.890	31.63	1.500	1.604	81.53	14.1 ± 0.7	4.234 ± 0.104	49.66 ± 1.04	37.68 ± 1.38
8	500	20	5.213	16.50	6.305	30.75	1.410	1.863	82.10	10.9 ± 0.6	4.280 ± 0.138	50.20 ± 1.36	41.08 ± 1.68
9	550	5	14.12	57.46	5.743	32.35	2.750	2.367	93.06	124 ± 2	13.14 ± 0.05	149.9 ± 0.54	3.20 ± 2.33
10	550	10	5.376	14.55	5.526	16.02	2.718	2.865	90.74	6.24 ± 0.51	4.878 ± 0.049	57.10 ± 0.52	52.12 ± 0.71
11	550	15	5.452	13.89	5.452	12.65	2.837	3.386	92.69	4.58 ± 0.47	5.054 ± 0.055	59.12 ± 0.55	55.60 ± 0.73
12	550	20	5.551	13.24	4.829	10.98	2.742	3.888	93.71	2.87 ± 0.48	5.202 ± 0.098	60.82 ± 0.90	58.83 ± 1.18
13	600	5	9.248	27.30	7.115	18.88	4.251	4.668	93.70	41.4 ± 0.5	8.666 ± 0.025	100.2 ± 0.36	4.74 ± 0.80
14	600	10	6.086	13.34	6.894	6.766	4.288	5.454	96.31	3.37 ± 0.21	5.861 ± 0.034	68.39 ± 0.36	65.96 ± 0.42
15	600	15	5.865	12.63	6.033	3.582	4.294	6.241	97.78	1.57 ± 0.22	5.734 ± 0.037	66.94 ± 0.37	66.09 ± 0.44
16	600	20	5.907	12.34	5.403	2.730	4.034	6.981	98.22	0.79 ± 0.25	5.802 ± 0.049	67.71 ± 0.48	67.54 ± 0.57
17	650	5	7.599	18.54	5.423	9.768	5.122	7.920	95.88	17.6 ± 0.4	7.286 ± 0.021	84.63 ± 0.22	69.80 ± 0.46
18	650	10	6.334	12.65	4.273	5.976	5.497	8.928	96.82	1.50 ± 0.23	6.132 ± 0.015	71.49 ± 0.16	71.49 ± 0.16
19	650	20	6.199	12.29	3.575	1.109	7.095	10.23	99.07	0.75 ± 0.21	6.142 ± 0.028	71.60 ± 0.27	71.47 ± 0.32
20	650	20	6.290	12.35	3.133	2.400	5.079	11.16	98.48	0.84 ± 0.21	6.194 ± 0.038	72.20 ± 0.37	71.99 ± 0.44
21	700	10	6.686	13.53	3.470	4.362	8.093	12.64	97.70	4.01 ± 0.23	6.532 ± 0.022	76.06 ± 0.23	73.08 ± 0.31

22	700	15	6.418	12.30	3.181	1.632	7.075	13.94	98.86	0.74 ± 0.27	6.345 ± 0.029	73.92 ± 0.30	73.80 ± 0.33
23	750	9	6.864	13.94	3.933	6.164	10.85	15.93	96.99	5.04 ± 0.26	6.657 ± 0.019	77.48 ± 0.20	73.60 ± 0.30
24	750	15	6.564	12.27	2.931	4.161	10.90	17.93	97.75	0.53 ± 0.17	6.416 ± 0.021	74.74 ± 0.22	74.80 ± 0.24
25	800	19	6.733	13.44	3.624	5.672	14.43	20.57	97.14	3.69 ± 0.17	6.541 ± 0.022	76.15 ± 0.23	73.46 ± 0.28
26	800	15	6.585	12.32	3.549	4.781	10.85	22.56	97.48	0.64 ± 0.16	6.419 ± 0.019	74.76 ± 0.20	74.73 ± 0.22
27	850	10	6.635	12.33	3.828	5.568	9.468	24.30	97.15	0.62 ± 0.42	6.446 ± 0.015	75.07 ± 0.14	–
28	850	15	6.573	12.39	3.457	5.353	7.604	25.69	97.22	0.80 ± 0.48	6.390 ± 0.025	74.44 ± 0.24	–
29	900	10	6.642	13.04	4.075	9.251	9.504	27.43	95.51	2.40 ± 0.46	6.344 ± 0.016	73.91 ± 0.15	–
30	900	16	6.512	13.05	3.576	9.450	8.741	29.04	95.33	2.41 ± 0.49	6.208 ± 0.020	72.35 ± 0.19	–
31	925	15	6.495	13.88	3.846	10.68	9.483	30.78	94.76	4.65 ± 0.44	6.155 ± 0.019	71.75 ± 0.18	–
32	950	15	6.721	14.57	4.261	10.47	11.00	32.79	95.03	6.58 ± 0.46	6.387 ± 0.019	74.40 ± 0.17	–
33	975	15	6.957	15.28	4.825	9.802	14.11	35.38	95.48	8.58 ± 0.46	6.643 ± 0.014	77.32 ± 0.13	–
34	1000	15	7.171	15.54	5.301	9.865	15.73	38.26	95.59	9.30 ± 0.48	6.855 ± 0.020	79.73 ± 0.17	–
35	1025	15	7.342	15.67	5.604	9.796	17.61	41.49	95.72	9.66 ± 0.48	7.028 ± 0.012	81.70 ± 0.12	–
36	1050	15	7.430	15.73	6.014	8.608	22.26	45.57	96.25	9.89 ± 0.45	7.151 ± 0.009	83.10 ± 0.09	–
37	1075	10	7.683	15.66	6.186	16.56	18.50	48.97	93.31	9.29 ± 0.52	7.170 ± 0.009	83.31 ± 0.09	–
38	1100	16	7.497	15.76	5.225	7.227	33.72	55.15	96.82	10.0 ± 0.6	7.259 ± 0.010	84.32 ± 0.09	–
39	1125	18	7.657	15.96	3.400	5.546	35.72	61.70	97.54	10.7 ± 0.5	7.468 ± 0.008	86.69 ± 0.08	–
40	1125	15	7.783	15.95	2.629	7.990	21.40	65.62	96.65	10.5 ± 0.4	7.522 ± 0.009	87.31 ± 0.08	–
41	1150	15	7.902	16.18	2.061	9.207	28.46	70.84	96.24	11.1 ± 0.5	7.605 ± 0.007	88.25 ± 0.07	–
42	1175	10	8.554	16.61	1.693	30.93	15.73	73.72	89.03	11.2 ± 0.5	7.615 ± 0.013	88.36 ± 0.13	–
43	1200	12	7.924	15.91	1.332	8.756	29.24	79.08	96.42	10.4 ± 0.5	7.641 ± 0.007	88.65 ± 0.07	–
44	1250	8	7.591	14.79	0.9814	5.111	66.61	91.29	97.68	7.46 ± 0.44	7.415 ± 0.008	86.10 ± 0.08	–
45	1300	8	9.030	15.21	1.161	54.32	26.76	96.20	81.95	6.08 ± 0.46	7.400 ± 0.016	85.93 ± 0.17	–
46	1550	5	48.45	40.63	1.402	1438	20.73	99.99	12.27	4.47 ± 1.26	5.946 ± 0.342	69.36 ± 3.82	–

[a] Cl/K offset of 6.0×10^{-5} applied to correct ages.
[b] $^{40}Ar_E$ /Cl = $6.17 \pm 0.10 \times 10^{-5}$.

Table 5
$^{40}Ar/^{39}Ar$ results for EH-29R-A4 K-feldspar (21.36 mg; $J = 0.006601$)

Step	T (C)	t (min)	$^{40}Ar/^{39}Ar$	$^{8}Ar/^{39}Ar$ $\times 10^{-3}$	$^{37}Ar/^{39}Ar$ $\times 10^{-4}$	$^{36}Ar/^{39}Ar$ $\times 10^{-3}$	moles ^{39}Ar $\times 10^{-15}$	% ^{39}Ar released	% $^{40}Ar*$	Cl/K^{a} $\times 10^{-4}$	$^{40}Ar*/^{39}Ar_{K}$	Conventional age (Ma)	Cl-corrected Age[b] (Ma)
1	450	10	37.35	121.7	9.161	52.22	7.551	0.4161	58.62	277 ± 4	21.89 ± 0.23	243.5 ± 2.3	38.83 ± 9.20
2	450	15	18.46	30.15	5.783	53.96	3.615	0.6153	13.46	22.2 ± 2.6	2.485 ± 0.233	29.35 ± 2.68	12.83 ± 3.43
3	450	9	15.06	33.98	50.32	39.04	1.450	0.6952	23.24	40.6 ± 12.3	3.499 ± 0.676	41.19 ± 7.79	10.13 ± 12.49
4	450	20	12.75	31.51	35.28	30.12	2.860	0.8527	30.03	38.4 ± 3.5	3.829 ± 0.292	45.03 ± 3.35	15.78 ± 4.51
5	500	7	10.88	48.01	33.38	15.80	6.329	1.201	56.88	91.5 ± 2.0	6.190 ± 0.178	72.25 ± 2.01	1.217 ± 3.812
6	500	10	8.598	23.17	33.81	12.34	5.520	1.506	57.34	24.5 ± 2.4	4.930 ± 0.177	57.78 ± 2.03	39.67 ± 2.82
7	500	15	8.826	22.56	42.54	13.38	5.793	1.825	54.97	22.3 ± 2.3	4.852 ± 0.229	56.87 ± 2.64	40.52 ± 3.23
8	500	20	9.167	19.08	35.48	13.45	5.672	2.137	56.39	12.6 ± 1.7	5.170 ± 0.156	60.54 ± 1.78	51.79 ± 2.18
9	550	5	16.07	47.95	33.34	13.19	12.11	2.805	75.59	92.7 ± 2.0	12.14 ± 0.10	139.1 ± 1.0	69.79 ± 3.30
10	550	10	7.582	17.40	38.28	7.405	11.08	3.415	70.85	11.1 ± 1.1	5.372 ± 0.103	62.86 ± 1.17	55.31 ± 1.42
11	550	15	7.691	15.95	37.71	7.319	10.93	4.018	71.59	7.13 ± 1.07	5.506 ± 0.092	64.40 ± 1.05	59.95 ± 1.26
12	550	33	8.037	15.63	34.16	7.866	14.59	4.822	70.80	5.97 ± 1.26	5.690 ± 0.085	66.52 ± 0.96	62.98 ± 1.24
13	600	6	9.325	25.78	35.68	7.916	12.36	5.502	74.67	34.1 ± 1.1	6.963 ± 0.103	81.07 ± 1.13	55.77 ± 1.73
14	600	10	6.750	14.66	35.37	1.912	13.30	6.235	91.30	6.38 ± 0.55	6.162 ± 0.109	71.93 ± 1.16	68.08 ± 1.30
15	600	17	6.779	13.61	32.31	1.819	15.68	7.100	91.74	3.52 ± 0.66	6.219 ± 0.117	72.58 ± 1.16	70.94 ± 1.37
16	600	20	8.666	14.77	31.14	8.067	12.34	7.780	72.23	3.48 ± 0.89	6.259 ± 0.163	73.04 ± 1.61	71.44 ± 1.91
17	650	5	9.393	20.31	35.44	5.332	13.99	8.550	82.99	20.3 ± 0.8	7.795 ± 0.090	90.52 ± 0.98	76.04 ± 1.29
18	650	10	6.953	13.01	33.91	1.053	18.06	9.545	95.20	2.24 ± 0.63	6.620 ± 0.076	77.16 ± 0.81	76.52 ± 0.89
19	650	15	6.966	13.14	31.96	1.096	17.75	10.52	95.03	2.60 ± 0.52	6.620 ± 0.099	77.16 ± 0.98	76.23 ± 1.15
20	650	20	7.063	12.85	30.05	0.8120	16.32	11.42	96.28	1.93 ± 0.61	6.800 ± 0.119	79.22 ± 1.15	78.81 ± 1.36
21	700	10	7.824	14.69	34.64	3.073	25.00	12.80	88.11	5.85 ± 0.42	6.893 ± 0.051	80.28 ± 0.53	76.86 ± 0.65

22	700	15	7.281	12.51	32.31	1.109	22.76	14.05	95.19	0.85 ± 0.37	6.931 ± 0.074	80.71 ± 0.74	81.14 ± 0.86
23	750	10	8.140	16.64	34.70	3.903	38.94	16.20	85.56	10.8 ± 0.3	6.965 ± 0.036	81.09 ± 0.37	73.84 ± 0.53
24	750	15	7.462	12.79	32.14	1.435	29.99	17.85	94.01	1.44 ± 0.30	7.016 ± 0.054	81.67 ± 0.53	81.64 ± 0.61
25	800	15	7.901	14.40	35.66	3.040	50.79	20.65	88.35	5.07 ± 0.42	6.980 ± 0.040	81.27 ± 0.42	78.45 ± 0.53
26	825	15	7.486	13.70	34.56	1.897	43.47	23.05	92.21	3.73 ± 0.34	6.903 ± 0.040	80.39 ± 0.40	80.39 ± 0.40
27	850	15	7.480	13.08	34.63	2.063	38.32	25.16	91.55	1.93 ± 0.38	6.848 ± 0.050	79.76 ± 0.50	79.76 ± 0.50
28	875	21	7.709	14.05	35.32	3.339	48.18	27.81	86.91	3.94 ± 0.50	6.700 ± 0.064	78.07 ± 0.68	78.07 ± 0.68
29	900	18	8.212	14.62	33.85	5.012	36.70	29.84	81.69	4.65 ± 0.36	6.709 ± 0.055	78.17 ± 0.55	78.17 ± 0.55
30	925	15	8.630	15.48	35.90	6.456	34.71	31.75	77.63	6.29 ± 0.36	6.700 ± 0.057	78.08 ± 0.59	78.08 ± 0.59
31	950	15	8.754	16.33	36.14	6.703	37.94	33.84	77.12	8.52 ± 0.42	6.751 ± 0.044	78.66 ± 0.43	78.66 ± 0.43
32	975	15	8.847	16.82	37.49	6.352	43.10	36.21	78.53	10.1 ± 0.6	6.948 ± 0.046	80.90 ± 0.47	80.90 ± 0.47
33	1000	15	8.389	17.04	38.81	4.365	50.16	38.98	84.36	11.7 ± 0.4	7.077 ± 0.051	82.37 ± 0.52	82.37 ± 0.52
34	1025	15	8.430	17.26	41.20	4.342	44.54	41.43	84.52	12.3 ± 0.5	7.125 ± 0.055	82.91 ± 0.58	82.91 ± 0.58
35	1050	19	8.117	17.90	46.51	3.199	69.85	45.28	88.09	14.7 ± 0.4	7.151 ± 0.036	83.20 ± 0.38	83.20 ± 0.38
36	1075	15	8.405	20.06	58.15	4.348	90.86	50.29	84.47	20.1 ± 0.5	7.100 ± 0.039	82.63 ± 0.40	82.63 ± 0.40
37	1100	17	8.760	21.63	65.95	5.353	111.8	56.45	81.71	23.9 ± 0.4	7.159 ± 0.042	83.30 ± 0.46	83.30 ± 0.46
38	1125	15	8.924	21.22	63.12	5.274	137.8	64.04	82.31	22.8 ± 0.6	7.346 ± 0.049	85.43 ± 0.54	85.43 ± 0.54
39	1150	15	9.043	20.84	57.92	5.139	172.9	73.57	82.98	21.8 ± 0.6	7.504 ± 0.043	87.22 ± 0.47	87.22 ± 0.47
40	1175	15	9.238	19.25	35.05	5.346	199.6	84.57	82.65	17.3 ± 0.5	7.636 ± 0.038	88.71 ± 0.42	88.71 ± 0.42
41	1200	15	9.989	18.74	23.22	8.000	142.4	92.42	76.10	14.5 ± 0.4	7.602 ± 0.045	88.33 ± 0.50	88.33 ± 0.50
42	1225	15	14.23	23.11	25.51	24.39	77.93	96.71	49.21	18.1 ± 0.7	7.004 ± 0.058	81.54 ± 0.62	81.54 ± 0.62
43	1250	15	30.85	39.69	47.54	80.69	29.05	98.32	22.65	34.7 ± 1.4	6.990 ± 0.206	81.38 ± 2.26	81.38 ± 2.26
44	1275	15	64.33	77.28	43.65	195.7	15.74	99.18	10.06	79.0 ± 2.6	6.475 ± 0.450	75.51 ± 4.66	75.51 ± 4.66
45	1300	15	179.2	174.6	61.92	586.4	8.072	99.63	3.291	145 ± 8	5.897 ± 2.027	68.89 ± 19.69	68.89 ± 19.69
46	1350	15	400.3	367.5	64.88	1343	6.764	99.99	0.8522	286 ± 20	3.411 ± 6.833	40.17 ± 67.01	40.17 ± 67.01

[a] Cl/K offset of 1.4×10^{-4} applied to correct ages.
[b] $^{40}Ar_E$ /Cl = $5.46 \pm 0.21 \times 10^{-5}$.

yield coherent age spectra that conform to profiles expected for diffusion loss. In an effort to increase resolution we performed four successive isothermal steps at each temperature for all samples. In doing so we discovered that sensible profiles could be estimated simply from ages yielded by the latter steps (Fig. 4e, Fig. 5e, Fig. 6e and Fig. 7e). However, elevated Cl/K values obtained for the lower temperature of these (< 500°C; Tables 2–5), indicate that correction for Cl-correlated $^{40}Ar_E$ is still required. As detailed in Harrison et al. (1994), the slope ($^{40}Ar_E/Cl$) of the array of $\Delta(^{40}Ar*/K)$ vs. $\Delta(Cl/K)$ values from successive isothermal steps is used in conjunction with the measured Cl/K ratio of each heating step to subtract contaminating Cl-correlated $^{40}Ar_E$ (i.e.; $^{40}Ar_R/K = {}^{40}Ar*/K - (^{40}Ar_E/Cl) \cdot (Cl/K)$) For the correction to be applicable, $\Delta^{40}Ar_R/K$ for successive isothermal steps must be negligible (i.e.; $\Delta(^{40}Ar*/K) \approx (^{40}Ar_E/Cl) \cdot \Delta(Cl/K)$). While this assumption appears adequate for most K-feldspars we have examined (Lovera et al., 1997), samples in the present study are somewhat problematic. Specifically, ages of the most affected steps are overcorrected when a York (1969) type regression is applied and undercorrected when the intercept of the regression is fixed at zero (see

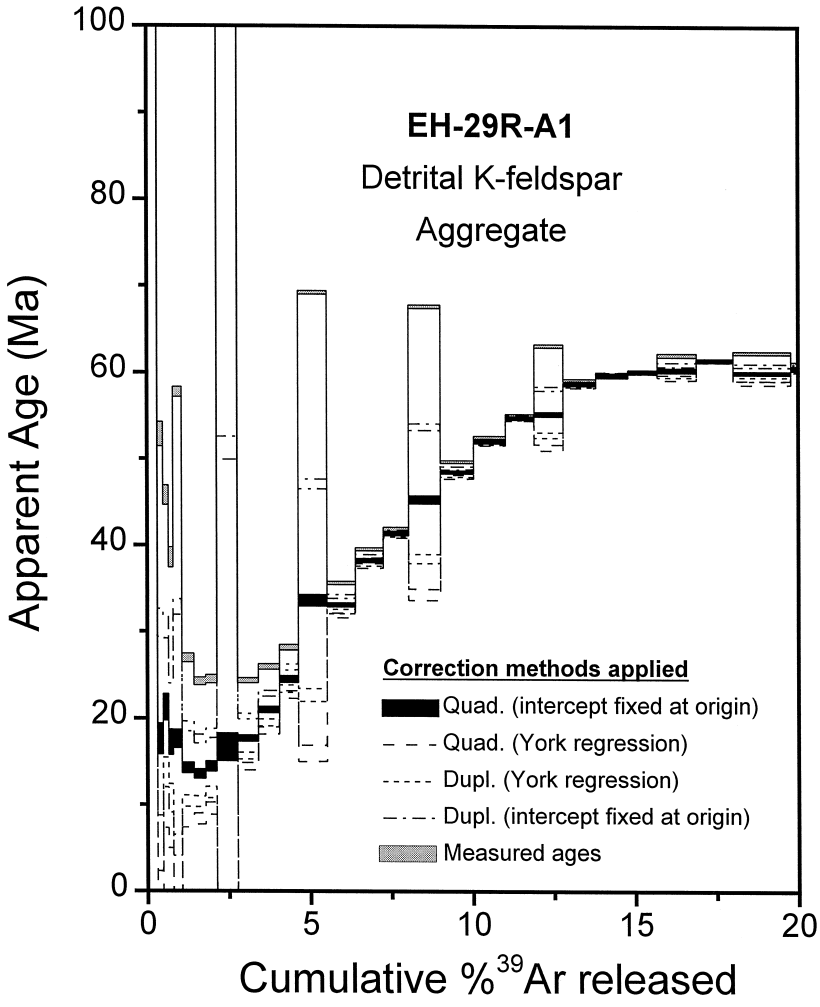

Fig. 8. Effect of different methods that can be applied to correct age spectra for Cl-correlated $^{40}Ar_E$. York regression and fixed intercept fitting routines discussed in Mahon (1996). Use of either two or four successive isothermal steps is discussed in the text.

Mahon, 1996 for a description of the regression algorithms). We attribute this phenomena to the pronounced gradients of in situ $^{40}Ar*$ that result from the youthful reheating event that create significant $\Delta^{40}Ar_R/K$ across the portion of ^{39}Ar release representing the isothermal quadruplicates.

To remediate this problem, we have investigated using an estimate of $\Delta(^{40}Ar_R/K)$ from the final pair of duplicate isothermal steps to obtain an improved estimate of $^{40}Ar_E/Cl$. Values of $\Delta(^{40}Ar*/K)$ from the first two steps were corrected according to:

$$\Delta\left(^{40}Ar*/K\right) = \Delta\left(^{40}Ar*/K\right)_{1-2} - \Delta\left(^{40}Ar_R/K\right)_{3-4} \quad (1)$$

where $\Delta(^{40}Ar*/K)_{1-2}$ is calculated from the difference between the first and second steps while $\Delta(^{40}Ar_R/K)_{3-4}$ is calculated from the difference between the third and fourth steps. Because $\Delta(^{40}Ar_R/K)_{3-4}$ is a negative quantity, $\Delta(^{40}Ar*/K)$ increases at a given value of Cl/K. The result is that values of $^{40}Ar_E/Cl$ now yield sensible results when the regression is forced through the origin, although highly overcorrected ages result when the York regression is applied (Fig. 8). Because the correction requires that the array of $\Delta(^{40}Ar*/K)$ vs. $\Delta(Cl/K)$ values pass through the origin, we have used $\Delta(^{40}Ar_R/K)$ corrections based upon the final two steps and fixed-intercept regression in determining $^{40}Ar_E/Cl$ to apply corrections for inclusion-derived $^{40}Ar_E$ in all the samples. The $\Delta(^{40}Ar*/K)$ vs. $\Delta(Cl/K)$ plots produced in this manner are shown in Fig. 4d, Fig. 5d, Fig. 6d and Fig. 7d while age spectra corrected for Cl-correlated $^{40}Ar_E$ are displayed in Fig. 4e, Fig. 5e, Fig. 6e and Fig. 7e. Values for $^{40}Ar_E/Cl$ yielded by the four samples are virtually identical ($5.4 \pm 0.9 \times 10^{-5}$) and within the range of previously reported values (Harrison et al., 1994). Although we believe that the approach described here provides the best and most robust estimate of $^{40}Ar_E/Cl$, we note that all other approaches yield similar estimates (Fig. 8).

4.3. Thermal modeling

Under the assumption of monotonic cooling, calculated thermal histories obtained from $^{40}Ar/^{39}Ar$ K-feldspar step-heating typically define a relatively narrow range of possible temperature–time condi-

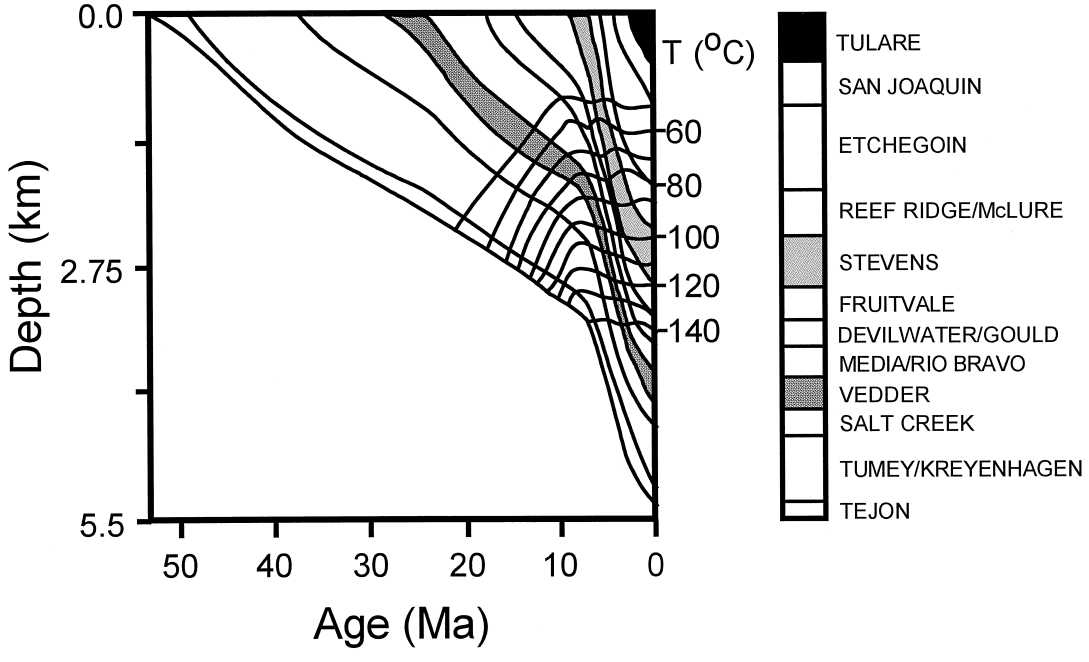

Fig. 9. Deposition and thermal histories of the North Coles levee oil field (modified from Wood and Boles, 1991).

tions (Lovera et al., 1997). When reheating is considered, however, the range of potential T–t histories capable of explaining the measured results expands significantly (e.g., Quidelleur et al., 1997). Thus in order to obtain a meaningful estimate of the thermal evolution at Elk Hills, we found it necessary to restrict the possible range of temperature–time histories as a function of depth to those that are consistent with the burial history experienced by the samples. Specifically we have adopted a strategy in which the input histories used to forward model the measured age spectrum were calculated using a conductive heat-flow model calibrated with a burial history model derived for the Elk Hills field.

In addition to specifying a framework for reheating histories during burial, it is also necessary to assume an initial ^{40}Ar concentration distribution within the K-feldspars requiring an estimate of the pre-depositional history of the grains. Although polygenetic samples precludes precise estimates of the samples previous history, failure to account for first-order effect could cause a small overestimation of the intensity of heating experienced during burial. We have assumed a source region cooling history in which temperature drops from ~ 300°C to < 150°C between 80 and 65 Ma. This history, which approximates that indicated by presently exposed basement in the Sierra Nevada (e.g., Harrison and Bé, 1983; Ryerson and Harrison, 1990), was then applied to each of the samples.

4.3.1. Burial history

Wood and Boles (1991) estimated the burial history of the North Coles Levee oil field (Fig. 9) by determining the rate of tectonic subsidence required to produce the observed sediment thickness after the depth dependent compaction and sediment loading was subtracted (e.g., Sclater and Christie, 1980). This reconstruction indicated a dramatic increase in subsidence rate during the middle to late Miocene (Fig. 9). Subsidence of ~ 54 m/m.y. preceded this period of rapid deposition, which peaked at > 600 m/m.y. during deposition of the Stevens sands at around 6 Ma. Subsequently, the general rate of subsidence decreased.

A subsidence model for the Elk Hills oil field was developed that is consistent with the age-depth relationship observed within well 934-29R. An additional constraint is that the present equilibrium temperature at a depth of 2005 m is ~ 95°C (Mark Wilson, pers. comm., 1996). The burial history for the horizons containing the four core samples from 934-29R, as well as cores from the Stevens zone (well 352X-3G, Fig. 1) corresponding to the sampled levels for the companion stable isotope study (Mahon et al., 1998), are shown in Fig. 10a. The Wood and Boles (1991) burial history assumes a depositional age of 6 Ma for the Stevens, the age of the Stevens' top from their plot (Fig. 9). We have used a marginally older age of 7 Ma to keep the model consistent with the subsidence history derived from older strata. Both values are consistent with the

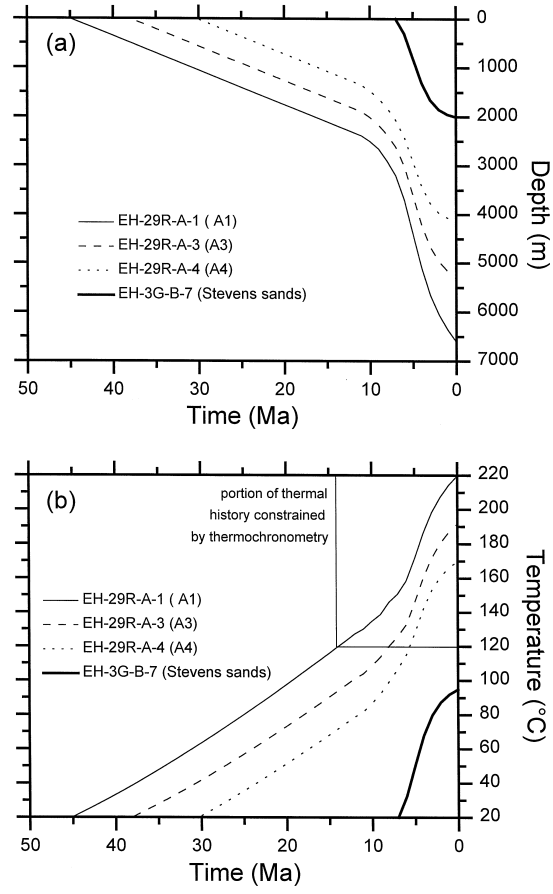

Fig. 10. (a) Burial history estimated for Elk Hills using data from Reid (1990a). (b) Estimated thermal history for depths corresponding to samples A1 to A4 from NPR-1 well 934-29R, Elk Hills. Also shown is the temperature evolution predicted for the Stevens sands interval used in Mahon et al. (1998).

assignment of Calloway (1990) of an upper Mohnian (6–10 Ma) deposition age for the Stevens at the location of our samples in the Main Body B of the Elk Hills shale member, the oldest of the three uppermost productive zones (Reid, 1990b). Because the other two zones are comprised of several hundred meters of sands and shales, about 1 m.y. of continued deposition at the rate appropriate for that time (>600 m/m.y.; Wood and Boles, 1991) is indicated.

4.3.2. Thermal model

Given the reasonably well-constrained burial history shown in Fig. 10a, we can use conductive heat flow theory to model the temperature evolution of any stratum as a function of time, assuming an initial thermal gradient. The solution to the problem of heat flow in a moving medium provides us with a simple analytical expression that describes our setting reasonably well. Eq. (2) gives the temperature distribution, $T(x)$, in a solid moving at a velocity $U(t)$ at any time, t, with an initial temperature of $T_0 = 20$°C at $x = 0$, and an initial temperature gradient of $\mathrm{d}T/\mathrm{d}t$ (Carslaw and Jaeger, 1959).

$$T(x) = T_0 + \frac{\mathrm{d}T}{\mathrm{d}x}x + (\kappa A_0 t/K) - \frac{\mathrm{d}T}{\mathrm{d}x}U(t)t + \frac{1}{2U(t)}\left(\frac{\mathrm{d}T}{\mathrm{d}x}U(t) - \frac{\kappa A_0}{K}\right) \times \left((x + U(t)t)\, e^{U(t)x/\kappa}\mathrm{erfc}\left(\frac{x + U(t)t}{2\sqrt{\kappa t}}\right) + (x - U(t)t)\, e^{U(t)x/\kappa}\mathrm{erfc}\left(\frac{x - U(t)t}{2\sqrt{\kappa t}}\right)\right) \quad (2)$$

Eq. (2) can be evaluated for any t using appropriate material properties for basin rocks (e.g., Issler and Beaumont, 1989). The values used are: thermal conductivity, $K = 2.0$ W/(m-°C); thermal diffusivity, $\kappa = 10^{-6}$ m^2/s, and heat generation, $A_0 = 0.3 \times 10^{-6}$ W/m^3. Three initial geothermal gradients of 30°/km, 35°/km, 40°/km (at $t = 0$) were used to generate input thermal histories for the MDD model. The predicted age spectra were then compared to the analytical results (Fig. 4e, Fig. 5e, Fig. 6e and Fig. 7e). Note that the model geothermal gradient changes over time due to the balance between the refrigerating effects of burial and heating due to radioactivity.

Synthetic age spectra calculated from the MDD model using input temperature–time histories corresponding to differing initial thermal gradients and constrained by the subsidence histories for the three levels (Fig. 10a) studied in well 934-29R are shown in Fig. 4e, Fig. 5e, Fig. 6e and Fig. 7e. Note that because of our focus upon the late Cenozoic burial history and the lack of relevance of the calculations to pre-depositional times, only the portion of the age spectra corresponding to the first 20% of ^{39}Ar release are shown. The input temperature–time paths used to calculate the age spectra in Fig. 4e, Fig. 5e, Fig. 6e and Fig. 7e are displayed in Fig. 4f, Fig. 5f, Fig. 6f and Fig. 7f. These curves are numerical solutions of Eq. (2) using a time step, Δt, of 1 m.y. Values for $U(t)$, obtained from the subsidence history for that time interval (from Fig. 10a), are entered at the start of each time interval, and $T(x)$, x, and $\mathrm{d}T/\mathrm{d}x$ are then computed.

5. Discussion

5.1. Thermal evolution at Elk Hills

The best-fit temperature histories resulting from differing assumptions regarding initial thermal gradient and constrained by the subsidence histories for the three levels (Fig. 10a) studied in well 934-29R are shown in Fig. 10b. The corrected ^{40}Ar/^{39}Ar age spectra for the detrital K-feldspars clearly show the effect of diffusive ^{40}Ar loss due to heating during burial in the basin (Fig. 4e, Fig. 5e, Fig. 6e and Fig. 7e). Although the youngest depositional age of any of the samples is ca. 30 Ma (i.e., A4), the Cl-corrected age spectrum yield effectively zero ages in the initial gas released (Fig. 7e). Similar relationships were obtained for the other three samples. Sample A1 yields apparent ages younger that the deposition age of ca. 45 Ma over the first 10% of gas release (Fig. 4e). Although A2 and A3 are separated by <1 m in the core, their age spectra are considerably different (Fig. 5e and Fig. 6e) with A2 apparently experiencing greater ^{40}Ar$*$ loss than A3. In part, this is explicable in terms of the calculated diffusion

parameters. A2 has a lower activation energy (46.4 kcal/mol) than that of A3 (52.8 kcal/mol), thus is expected to lose a greater fraction of $^{40}Ar*$ for a given heating history. However, as noted earlier, A2 was a non-ideal separate that appears to have experienced significant recrystallization and thus, diffusion is not likely to have been the rate limiting step in argon transport. Consequently, we do not consider the results of sample A2 further in our attempts to model the thermal history of the basin.

The utility of using the laboratory diffusion parameters and age spectrum to constrain the basin subsidence thermal history is well-illustrated using sample A3. Comparing the age spectra predicted for initial thermal gradients of 30°C/km, 35°C/km, and 40°C/km with the Cl-corrected age spectrum for this sample (Fig. 6e) shows that the best fit is obtained by using a value close to 35°C/km. The higher gradient results in too much $^{40}Ar*$ release while the lower gradient does not generate temperatures sufficiently high to produce argon loss. Although this model appears to degas too much $^{40}Ar*$ in the smallest domains (Fig. 6e), it is likely that $^{40}Ar_E$ in the first several percent of ^{39}Ar release from this sample has been underestimated by the correction applied for Cl-correlated excess argon. Note that a 35°C/km gradient also yields the best fit for the deepest sample (A1; Fig. 4e and f). In contrast, the shallowest sample (A4) experienced relatively minor $^{40}Ar*$ loss and can be well modeled assuming an initial gradient of 40°C/km (Fig. 7e). This is not surprising as the predicted gradients for A1 and A3 depths evolve to values of 41°C/km and 38°C/km, respectively, at the time of deposition of A4. Therefore, a value of 40°C/km for the initial geotherm for A4 is consistent with those derived from analysis of A1 and A3.

The results for samples A1, A3, and A4 are consistent with present day temperatures that are ~20°C higher than the static measured temperature, T_{SM}. T_{SM} for A1 is 200°C whereas the predicted equilibrium formation temperature from the best fit to the $^{40}Ar/^{39}Ar$ results is ~220°C. Samples A3 and A4 have T_{SM} and estimated equilibrium formation temperatures from thermochronometry of 170°C vs. 190°C and 150°C vs. 170°C respectively. A discrepancy between measured borehole temperature and equilibrium formation temperature is common in oil wells due to a number of factors (Drury, 1984; Corrigan and Bergman, 1996). Drill stem and productions tests below 5000 m in 934-29R produced a significant amount of gas (Fishburn, 1990). Because gas expansion into the borehole results in cooling of the surrounding formation, static temperature measurements are considered a lower estimate of the equilibrium formation temperature. Therefore, the value predicted by thermochronological analysis is expected to exceed T_{SM}.

Having established a reasonable thermal evolution model for depths between 4.12 and 6.61 km in the 934-29R well, we can extrapolate the results to predict the temperature histories at shallower intervals, including those in the Stevens zone. Fig. 10b illustrates the best fit temperature histories for the intervals corresponding to A1, A3, and A4, together with the thermal evolution predicted for a horizon deposited at 7 Ma and currently at a depth of 2 km. This approximates the present depth of the Stevens sands from well 352X-3G from which samples EH-3G-B-6 through EH-3G-B-8, used in our companion study (Mahon et al., 1998), were obtained. The present-day temperature predicted by our model for a depth of 2005 m is identical to the measured equilibrium temperature of 95°C (Mark Wilson, pers. comm., 1996).

Our results also have some bearing on the question of the hydrocarbon potential of pre-Miocene rocks at Elk Hills. Because bottom hole temperatures appear to underestimate the formation temperature by about 20°C, we estimate that the current true temperatures for A1 and A4 are 220°C and 170°C respectively. Assuming depositional ages for A1 and A4 of 45 and 30 Ma, respectively, and a constant depositional rate, both these horizons have experienced temperatures well above that appropriate for petroleum formation (Hunt, 1979). Even modifying the burial history such that both levels experience ~60% of their subsidence over the past 10 m.y. still places them in temperature–time conditions greater than those necessary for the preservation of petroleum. Thus there appears to be little potential for the early Oligocene deposits in 934-29R to contain substantial quantities of liquid hydrocarbons in this region of Elk Hills. By extrapolating thermal and depositional histories to the Miocene–Oligocene boundary (~24 Ma), the unit deposited at that time

has a current temperature of ~148°C and an 'effective' depositional age of 14 Ma (i.e., extrapolating the present depositional rate back in time). This temperature is close to the upper limit of petroleum stability suggesting little potential for large quantities of oil reservoired in Oligocene strata. In fact, the oldest productive interval found at Elk Hills is the Carneros sandstone (Nicholson, 1990) of early Miocene age (18–21 Ma: Calloway, 1990).

5.2. Significance of $^{40}Ar_E/Cl$

The remarkable similarity of $^{40}Ar_E/Cl$ ratios shown in Fig. 4d, Fig. 5d, Fig. 6d and Fig. 7d has implications for the evolution of the pore fluid within the basin. The average value of the four samples of $5.4 \pm 0.9 \times 10^{-5}$ is within the range of previously reported values (Harrison et al., 1994). The uniformity of these results appears to require that the incorporation of $^{40}Ar_E$ bearing brines have occurred during burial rather than during deuteric processes that predate deposition. If so, we can further infer that the $^{40}Ar_E/Cl$ ratio of the pore fluid was essentially constant across the vertical distance of 2.5 km that separated samples A1 and A4 at the time the fluid inclusions formed.

Direct measurement of $^{40}Ar_E/Cl$ in fluids extracted from production wells is complicated by the exsolution of fluid and gas phases brought from depth. However, a lower bound can be placed on the fluid $^{40}Ar_E/Cl$ by making reasonable assumptions regarding the behavior of the gas/fluid system during sample collection (Tom Torgerson, pers. comm., 1997). Data obtained from the Point of Rocks member, immediately below our deepest sample (Fig. 2), indicate an $^{40}Ar_E/Cl$ of 2×10^{-5}. In the shallower Carneros sandstone, the value is 7×10^{-6}. The Point of Rocks value is within a factor of three of our observed value of $5.4 \pm 0.9 \times 10^{-5}$ and probably equivalent within uncertainty given the assumptions required to derive the estimate from the well measurements. The similarity of our results with that of the modern fluids suggests that unless $^{40}Ar_E/Cl$ remained constant throughout the basin's history, the inclusion hosted brines must have been incorporated recently when temperatures were close to peak values rather than when the samples were at shallower levels.

Assuming an average pore fluid chlorine content of 0.0035 M (Kharaka et al., 1973), the observed fluid $^{40}Ar_E/Cl$ of $5.4 \pm 0.9 \times 10^{-5}$ implies an $^{40}Ar_E$ content in the fluid of 2×10^{-7} M. However, the measured porosity (6%; Appendix A), estimated bulk rock potassium content (2%; Appendix A), and average K-Ar feldspar age (ca. 80 Ma; Fig. 4a, Fig. 5a, Fig. 6a and Fig. 7a) would require complete degassing of the K-feldspars in a closed system in order to yield a comparable value of $^{40}Ar_E/Cl$. The fact that the feldspars preserve their ~80 Ma source ages requires a significant addition of $^{40}Ar_E$ into the basin, presumably through a high basal flux (Torgerson et al., 1989). The fact that $^{40}Ar/^{4}He$ ratios are observed to increase with depth in Elk Hills production wells (Mack Kennedy, pers. comm., 1997) suggests a high basal flux of ^{40}Ar.

6. Conclusions

We have revisited the use of $^{40}Ar/^{39}Ar$ K-feldspar thermochronometry to constrain sedimentary basin thermal histories in light of the development of the multi-diffusion domain model and a method to correct for Cl-correlated excess ^{40}Ar. $^{40}Ar/^{39}Ar$ thermochronological results from detrital K-feldspars recovered from a deep well in the Naval Petroleum Reserve Number 1, Elk Hills, California, are consistent with a broadly linear heating history due to burial throughout the early and middle Miocene. Between 9–6 Ma, the basin heating rate increases significantly. This result is supported by the observation of enhanced subsidence that began around 10 Ma and peaked between 5 and 7 Ma. The Stevens sands, a prolific petroleum producer that is the focus of the companion ion microprobe study of the cementation history (Mahon et al., 1998), were deposited at ~7 Ma. The thermal model developed in this study can be used to predict the temperature history of levels corresponding to the Stevens sands and assist in assessing the porosity evolution of the reservoir. Our results appear to preclude the likelihood of a large liquid hydrocarbon resource in pre-Miocene deposits at Elk Hills as the temperature–time conditions are expected to have greatly exceeded those appropriate for the preservation of liquid hydrocarbons.

Acknowledgements

We thank the Department of Energy, Bechtel Petroleum Operations Incorporated (BPOI), and the Chevron staff at NPR-1 for providing us with core materials and for their gracious assistance. In particular, we wish to thank Mark Wilson and George McJanet for sharing their expertise of the oil field with us. Helpful reviews were obtained from Jim Dunlap, Jeff Corrigan, and Bill Clendenen. Funding for this research was provided by a grant from the Department of Energy Office of Basic Sciences.

Appendix A. Sample descriptions

Four core segments of Eocene to Oligocene rocks from NPR-1 well 934-29R were obtained from units locally known as the Oligocene Phacoides sandstone (EH-29R-A-4 at 4121 m), the Oligocene Oceanic sandstone (EH-29R-A-2 and EH-29R-A-3 both at 5316 m), and the Eocene Point of Rocks (EH-29R-A-1 at 6607 m). Static temperatures measured for these three horizons are, with increasing depth, 150°, 170°, and 200°C (Fishburn, 1990).

A.1. EH-29R-A-1 (A1)

The Point of Rocks sandstone of the Kreyenhagen formation (Eocene) is found in well 934-29R from drill depths of 6596–6977 m and is a moderately well sorted, fine to coarse grained arkosic sandstone (Fishburn, 1990). Average porosity is 6% and permeability < 1 md. Minor amounts of gas were also found (Fishburn, 1990). The core EH-29R-A-1 (A1) is from a drill depth of 6607. Petrographic observation indicates 50% quartz, 30% feldspar (subequal plagioclase and potassium feldspar), $\sim$ 15% carbonate cement, and lesser amounts of muscovite and altered biotite. Quartz and feldspar grains are generally 200–300 μm in size with a few larger grains.

A.2. EH-29R-A-2 and EH-29R-A-3 (A2, A3)

The Oceanic sandstone of the Tumey formation (Oligocene) occurs at depths of 5212 to 5514 m in well 934-29R. The upper portion of the Oceanic sandstone is comprised of volcanic ash and volcanic-rich sand and lies unconformably on the lower sandstone unit. The lower portion is comprised of gray to white, very-fine to medium grained graywacke with a majority of the clasts consisting of andesite debris. Porosity varies from 4 to 9% and permeability is < 1 md (Fishburn, 1990). Core EH-29R-A-2 (A2) comes from a drill depth of 5316.5 m and EH-29R-A-3 (A3) a depth of 5316.2 m. A2 contains 50% quartz, subequal amounts of plagioclase and K-feldspar (typically 200 μm in size), and minor amounts of biotite and muscovite. The biotite and plagioclase are highly altered and clay minerals are abundant. A3 is similar to A2 with the addition of some lithic fragments and some feldspar and quartz grains up to 500 μm (Fishburn, 1990).

A.3. EH-29R-A-4 (A4)

The Phacoides sandstone of the Temblor formation (Oligocene) is intersected between 3911 to 4514 m in well 934-29R. It consists of fine- to medium-grained arkosic, blocky massive sandstone that is interbedded at its base with shale layers containing minor amounts of pyrite, having low porosity (2 to 14%) and low permeability (< 1 md) (Fishburn, 1990). Relic fossils and calcareous fossil debris are common. The core EH-29R-A-4 (A4) was recovered from a depth of 4121 m. The rock is $\sim$ 65% quartz with much less feldspar, which is mostly plagioclase. Biotite and muscovite are subequal in abundance and the biotite is not as altered as in the other samples. The grain size ranges from 150 to 250 μm.

References

Barton, M.D., Battles, D.A., Bebout, G.E., Capo, R.C., Christensen, J.N., Davis, S.R., Hanson, R.B., Michelsen, C.J., Trim, H.E., 1988. Mesozoic contact metamorphism in the western United States. In: Ernst, W.G. (Ed.), Metamorphism and Crustal Evolution of the Western United States: Rubey Volume VII. Prentice Hall, Englewood Cliffs, NJ, pp. 110–178.

Bent, J.V.B., 1988. Paleotectonics and provenance of Tertiary sandstones of the San Joaquin basin, California. Studies of the Geology of the San Joaquin Basin. SEPM, Los Angeles, CA, pp. 109–120.

Calloway, D.C., 1990. Organization of stratigraphic nomenclature for the San Joaquin basin, California. Structure, Stratigraphy and Hydrocarbon Occurrences of the San Joaquin Basin, California. SEPM and AAPG, Bakersfield, CA, pp. 5–22.

Carslaw, H.S., Jaeger, J.C., 1959. Conduction of Heat in Solids, 2nd edn. Oxford Univ. Press, 510 pp.

Cebula, G.T., Kunk, M.J., Mehnert, H.H., Naeser, C.W., Obradovich, J.D., Sutter, J.F., 1986. The Fish Canyon Tuff, a potential standard for the $^{40}Ar-^{39}Ar$ and fission-track dating methods. Terra Cognita 6, 139–140.

Corrigan, J., Bergman, S., 1996. Thermal modeling and interpretation of thermal indicator data. AAPG 1996 Annual Convention —Official Program, p. A30.

Dickinson, W.R., 1974. Plate tectonic and sedimentation. Tectonics and Sedimentation, Soc. Econ. Paleont. Mineral. Spec. Paper 22, pp. 1–27.

Drury, M.J., 1984. On a possible source of error in extracting equilibrium formation temperatures from borehole BHT data. Geothermics 13, 175–180.

Fishburn, M.D., 1990. Results of deep drilling: Elk Hills field, Kern County, California. Structure, Stratigraphy and Hydrocarbon Occurrences of the San Joaquin Basin, California. SEPM and AAPG, Bakersfield, CA, pp. 157–168.

Friedman, I., O'Neil, J.R., 1977. Compilation of stable isotope fractionation factors of geochemical interest. In: Fleischer, J.M. (Ed.), Data of Geochemistry, 6th edn., U.S.G.S. Prof. Paper 440-KK, 12 pp.

Gleadow, A.J.W., Duddy, I.R., Lovering, J.F., 1983. Fission track analysis: a new tool for the evaluation of thermal histories and hydrocarbon potential. Aust. Petrol. Explor. Assoc. J. 23, 93–102.

Graham, S.A., Williams, L.A., 1985. Tectonic, depositional, and diagenetic history of Monterey Formation, central San Joaquin basin, California. AAPG Bull. 69, 385–411.

Harrison, T.M., Bé, K., 1983. $^{40}Ar/^{39}Ar$ thermochronology of detrital microcline from the southern San Joaquin basin, California: an approach to determining the thermal evolution of sedimentary basins. Earth Planet Sci. Lett. 64, 244–256.

Harrison, T.M., Burke, K., 1988. $^{40}Ar/^{39}Ar$ thermochronology of sedimentary basins using detrital K-feldspars: Examples from the San Joaquin Valley, California, Rio Grande Rift, New Mexico, and North Sea. In: Naeser, N., McCulloh, T. (Eds.), Thermal History of Sedimentary Basins Springer-Verlag, pp. 141–155.

Harrison, T.M., Heizler, M.T., Lovera, O.M., 1993. In vacuo crushing experiments and K-feldspar thermochronometry. Earth Planet Sci. Lett. 117, 169–180.

Harrison, T.M., Heizler, M.T., Lovera, O.M., Chen, W., Grove, M., 1994. A chlorine disinfectant for excess argon released from K-feldspar during step-heating. Earth Planet Sci. Lett. 123, 95–104.

Hayes, M.J., Boles, J.R., 1993. Evidence of meteoric recharge in the San Joaquin basin, California provided by isotope and trace element chemistry of calcite. Marine and Petroleum Geology 10, pp. 135–144.

Heizler, M.T., Harrison, T.M., 1991. The heating duration and provenance ages of rocks in the Salton Sea Geothermal Field, southern California. J. Vol. Geotherm. Res. 46, 73–97.

Hunt, J.M., 1979. Petroleum Geochemistry and Geology. W.H. Freeman, San Francisco, CA, 617 pp.

Issler, D.R., Beaumont, C., 1989. A finite element model of the subsidence and thermal evolution of extensional basins: application to the Labrador continental margin. In: Naeser, N.D., McCulloh, T.H. (Eds.), Thermal History of Sedimentary Basins: Methods and Case Histories. Springer-Verlag, New York, pp. 239–268.

Jones, C.L., Gillespie, J.M., 1995. Listric normal faults from the Plio-Pleistocene section at the North Coles Levee oil fields: a response to post-Pliocene growth of the Elk Hills anticline. AAPG Bull. 79, 589.

Kharaka, Y.K., Berry, F.A.F., Friedman, I., 1973. Isotopic composition of oil field brines from Kettleman Dome, California, and their geologic implications. Geochim. Cosmochim. Acta 37, 1899–1908.

Lovera, O.M., Richter, F.M., Harrison, T.M., 1989. $^{40}Ar/^{39}Ar$ geothermometry for slowly cooled samples having a distribution of diffusion domain sizes. J. Geophys. Res. 94, 17917–17935.

Lovera, O.M., Richter, F.M., Harrison, T.M., 1991. Diffusion domains determined by ^{39}Ar release during step heating. J. Geophys. Res. 96, 2057–2069.

Lovera, O.M., Grove, M., Harrison, T.M., Mahon, K.I., 1997. Systematic analysis of K-feldspar $^{40}Ar/^{39}Ar$ step-heating experiments: I. Significance of activation energy determinations. Geochim. Cosmochim. Acta 61, 3171–3192.

Lowell, D., 1972. Spitsbergen Tertiary orogenic belt and the Spitsbergen fracture zone. GSA Bull. 83, 3091–3102.

MacPherson, B.A., 1977. Sedimentation and trapping mechanism in upper Miocene Stevens and older turbidite fans of southeastern San Joaquin Valley, California. AAPG Bull. 62, 2243–2274.

Maher, J.C., Carter, R.D., Lantz, R.J., 1975. Petroleum geology of Naval Petroleum Reserve No. 1, Elk Hills, Kern County, California. USGS Prof. Paper 912, 109 pp.

Mahon, K.I., 1996. The New 'York' regression: Application of an improved statistical method to geochemistry. Int. Geol. Rev. 38, 293–303.

Mahon, K.I., Harrison, T.M., McKeegan, K.D., 1998. The thermal and cementation histories of a sandstone petroleum reservoir, Elk Hills, California. Part 2: In situ oxygen and carbon isotopic results. Chem. Geol. 152, 257–271.

Mattinson, J.M., 1978. Age, origin, and thermal histories of some plutonic rocks from the Salinian block of California. Contrib. Mineral Petrol. 67, 233–245.

McJanet, G.S., 1993. Overview of geology, production, and reservoirs at Elk Hills. AAPG Bull. 77, 708.

Milliken, M.D., Deutsch, H., McJanet, G.S., 1993. Structurally controlled Miocene deep sea channels of the Stevens zone, Elk Hills field, Kern County, California. AAPG Bull. 77, 709.

Nicholson, G.E., 1990. Structural overview of Elk Hills. Structure, Stratigraphy and Hydrocarbon Occurrences of the San Joaquin Basin, California. SEPM and AAPG, Bakersfield, CA, pp. 133–140.

Quidelleur, X., Grove, M., Lovera, O.M., Harrison, T.M., Yin, A., Ryerson, F.J., 1997. The thermal evolution and slip history of the Renbu Zedong Thrust, southeastern Tibet. J. Geophys. Res. 102, 2659–2679.

Reid, S.A., 1990a. Elk Hills field overview. Structure, Stratigra-

phy and Hydrocarbon Occurrences of the San Joaquin Basin, California. SEPM and AAPG, Bakersfield, CA, pp. 131–132.

Reid, S.A., 1990b. Trapping characteristics of upper Miocene turbidite deposits, Elk Hills field, Kern County, California. Structure, Stratigraphy and Hydrocarbon Occurrences of the San Joaquin Basin, California. SEPM and AAPG, Bakersfield, CA, 141–156.

Richter, F.M., Lovera, O.M., Harrison, T.M., Copeland, P., 1991. Tibetan tectonics from a single feldspar sample: an application of the $^{40}Ar/^{39}Ar$ method. Earth Planet. Sci. Lett. 105, 266–276.

Ryerson, F.J., Harrison, T.M., 1990. Degassing of argon from microcline within the thermal aureole of the Obsidian Dome Conduit, Long Valley Caldera, California: Thermal constraints on emplacement. J. Geophys. Res. 95, 2781–2792.

Sclater, J.G., Christie, P.A.F., 1980. Continental stretching: an explanation of the post-mid-Cretaceous subsidence of the central North Sea basin. J. Geophys. Res. 85, 3711–3739.

Teichmüller, M., 1958. Métamorphisme du charbon et prospection du pétrole. Rev. Ind. Minérale Numero Special, 1–15.

Tieh, T.T., Berg, R.R., Popp, R.K., Brasher, J.E., Pike, J.D., 1986. Deposition and diagenesis of upper Miocene arkoses, Yowlumne and Rio Viejo fields, Kern County, California. AAPG Bull. 70, 953–969.

Torgerson, T., Kennedy, B.M., Hiyagon, H., Chiou, K.Y., Reynolds, J.H., Clarke, W.B., 1989. Argon accumulation and the crustal degassing flux of ^{40}Ar in the Great Artesian Basin, Australia. Earth Planet. Sci. Lett. 92, 43–56.

Wilson, M.L., McJanet, G.S., 1993. Main Body B-Western 31S waterflood, Elk Hills field, Kern County, California. AAPG Bull. 77, 721.

Wood, J.R., Boles, J.R., 1991. Evidence for episodic cementation and diagenetic recording of seismic pumping events, North Coles Levee, California, USA. Appl. Geochem. 6, 509–521.